nature communications

Article

https://doi.org/10.1038/s41467-025-64404-z

Fundamental role of spatial positioning of *Mycobacterium tuberculosis* in mycobacterial survival in macrophages

Received: 24 November 2022

Accepted: 12 September 2025

Published online: 23 October 2025

Check for updates

Shivani Sahu[1,6], Navin Baid[1,6], Deepali Aggarwal[1,2], Ankita Sharma[1,2], Manisha Gun[1], Sahanawaz Molla[3], Anunay Sinha[1,4], Ambey Prasad Dwivedi[1,4], Amit Tuli[1,2], Mahak Sharma[5], Sanjeev Khosla[1,2,4], Varadharajan Sundaramurthy[3] & Ashwani Kumar[1,2]

Mycobacterium tuberculosis is a model intracellular pathogen. The spatial-localization of *M. tuberculosis* inside macrophages is poorly defined. Here, we determine the spatial-localization of *M. tuberculosis* inside macrophages with reference to the nucleus. Few *M. tuberculosis* cells are perinuclear, while most are peripheral. Perinuclear *M. tuberculosis* are transported to lysosomes, have low Adenosine Triphosphate/Adenosine Diphosphate, are non-replicating, and tolerate front-line anti-tubercular medicines. *M. tuberculosis* pathogenicity determines its spatial location. Virulent *M. tuberculosis* strains are peripheral. However, avirulent *M. tuberculosis* strains or attenuated deletion mutants are transported to lysosomes in the perinuclear area. Early Secreted Antigenic Target-6 and Culture Filtrate Protein-10 play a critical role in inhibiting mycobacterial transport to the perinuclear space. Induction of centripetal transport of pathogenic *M. tuberculosis*-laden cargoes to perinuclear region enhances *M. tuberculosis*'s delivery to the lysosomes and reduces mycobacterial growth. Interferon-γ directs *M. tuberculosis* to lysosomes by modulating their perinuclear localization. Interferon-γ upregulates Transmembrane protein 55B and JNK-interacting protein 4 via transcription factor EB. Increased transmembrane protein 55B and JNK-interacting protein 4 levels tether *M. tuberculosis*-laden cargoes to the dynein motor, causing their perinuclear delivery to lysosomes. These findings shed light on how mycobacterial metabolism, reproduction, and drug susceptibility are connected to virulence-guided spatial localization.

Mycobacterium tuberculosis (Mtb) is an obligate intracellular pathogen that causes tuberculosis and kills millions of people annually[1]. Mtb primarily infects macrophages. It typically resides in phagosomes and autophagosomes[2,3], although it also escapes to cytoplasm[4]. The fate of Mtb within phagosomes/autophagosomes is closely associated with their maturation and fusion with lysosomes, while those escaping to the cytoplasm have been studied less. Phagosome maturation is guided by a series of exchanges of Ras-associated binding (Rab) GTPases[5]

[1]CSIR-Institute of Microbial Technology, Chandigarh, India. [2]Academy of Scientific and Innovative Research, Ghaziabad, India. [3]National Centre for Biological Sciences, Tata Institute of Fundamental Research, Bangalore, Karnataka, India. [4]Center for DNA Fingerprinting and Diagnostics, Hyderabad, Telangana, India. [5]Indian Institute of Science Education and Research, Mohali, Punjab, India. [6]These authors contributed equally: Shivani Sahu, Navin Baid.
e-mail: ashwani.kumar02@csir.res.in; ashwanik@imtech.res.in

and sequential modifications of membrane lipids[6,7]. These events facilitate the fusion of phagosomes with lysosomes, wherein pathogens are killed[8] and can be aided by cytokines like interferon-gamma (IFN-γ)[9]. Mtb inhibits phagosome maturation and avoids the bactericidal and degradative action of lysosomes. Virulent Mtb inhibits several key trafficking events upon phagocytosis, including phagosome maturation[3,8,10], phagosome-lysosome fusion, and its acidification[11]. Avirulent Mtb is attenuated to inhibit the maturation of phagosomes. The avirulent strain (MtbH37Ra) derived from parent virulent strains (MtbH37Rv) grows 100-fold less in guinea pigs[12] and ten-fold less in macrophages[13,14].

Heterogeneity amongst mycobacterial cells residing in different granulomas of the same lung is well recognized. It is known to affect the efficacy of the drugs and modulate the immune response[15–17]. However, the mycobacterial spatial positioning inside the macrophage and its relationship with mycobacterial virulence have remained largely ignored. Three problems compound this issue: (i) heterogeneity in the shape of macrophages, (ii) variability in the number of Mtb in a cell, and (iii) heterogeneity of distribution of Mtb cells in different organelles, namely, phagosome, phagolysosome, autophagosome, autolysosome and cytoplasm. Recently, micropatterning was employed to address the issue of heterogeneity of macrophage shape[18]. Several recently developed reporter strains have emphasized the heterogeneity in mycobacterial cells during infection. These include heterogeneity in intracellular pH[19], intracellular Cl^-[20], MSH/MSSM[21], rate of replication[22], NADH/NAD[23], ATP/ADP[24], etc. However, the metabolic state, replication status, and drug tolerance vis à vis the spatial localization of Mtb have not been analyzed.

In this study, we have defined the spatial localization of Mtb with respect to the nucleus inside the macrophages. We have explored whether virulence dictates spatial localization of Mtb inside the macrophages and if it affects the mycobacterial survival inside macrophages. We have also characterized the effect of variable subcellular localization on the metabolic state of Mtb, replication rate, and drug tolerance. We have also analyzed whether changing mycobacterial subcellular localization through genetic means or signaling molecules affects Mtb's intracellular survival and the molecular pathway involved therein.

Results

Defining the spatial localization of mycobacteria in macrophages

Mtb may alter the spatial localization of cargoes harboring it or escape from them into the cytoplasm to improve its survival. However, whether the spatial localization of Mtb influences its intracellular survival is poorly defined. There are several ways to define the subcellular localization of an organelle[25–27]. These approaches orient organelles relative to the nucleus or Pericentrin. Since the subcellular localizations of Mtb-laden phagosomes and cytoplasmic Mtb are unknown, we characterized the localization of Mtb in reference to the nucleus. As defined earlier for positioning of lysosomes[25,27], we drew concentric rings from the nucleus at 3 μm and 6 μm and measured mycobacterial fluorescence intensity within these rings to determine the perinuclear index. These concentric rings are smaller than used in earlier studies examining HeLa cells, where concentric rings of 5 μm and 10 μm were used as the THP-1 macrophages (400–1000 μm^2) are smaller than the HeLa cells (800–2500 μm^2). Nuclear fluorescence was excluded, and peripheral ($I > 6$) and perinuclear ($I < 3$) fluorescence of Mtb were normalized using whole cell fluorescence (I_{total}). The perinuclear index was calculated as $I < 3 - I > 6$ (Fig. 1a). In this method, positive values indicate closer localization of Mtb to the nucleus, while negative values indicate a peripheral Mtb localization. In an independent measure, we have recently defined fractional distance as a method for defining the spatial localization of lysosomes in cells[28]. Herein, we adapted this method to define the spatial localization of Mtb. In this approach, a line is drawn from the nucleus to the cell's periphery. Next, the plot profile tool extracts all lysosomal/Mtb fluorescence intensities and distance values along the line. The distance of the lysosomes/Mtb cell from the nuclear membrane is transformed to a fractional distance by dividing all the values by the line's total distance (Fig. 1b). In this method, the distance of Mtb cells from the nucleus ranges from 0 to 1. A smaller fractional distance indicates perinuclear localization of Mtb cells, while a higher value (closer to 1) suggests that Mtb cells are peripheral.

Mycobacterium actively modulates its retrograde transport to avert delivery to the lysosomes

To analyze whether Mtb modulates its subcellular localization, we infected THP-1 monocyte-derived macrophages with live and heat-killed MtbH37Rv cells. THP-1 macrophages were infected with Mtb at an MOI of 1:10. In order to get an accurate measurement of the spatial organization of Mtb within the cell; we excluded macrophages harboring more than five bacilli from the analysis. This is critical as macrophages with a larger number of bacilli show crowding within the limited cytoplasmic area, thereby influencing the relative distance measurements. We have also excluded the macrophages with more than one nucleus. We observed that most live Mtb cells localized away from the nucleus in the cell periphery, while most heat-killed Mtb cells localized in close proximity to the nucleus (Fig. 1c). We measured the perinuclear index and fractional distance to quantify the subcellular localization of live and heat-killed Mtb cells. We observed that the perinuclear index of live Mtb was significantly lower than the heat-killed bacilli (Fig. 1d). Fractional distance analysis revealed that live Mtb cells have higher fractional distances compared to heat-killed Mtb cells (Fig. 1e). We also measured the distance of Mtb from the nucleus and normalized it with the cell perimeter. Again, we observed that live Mtb cells reside towards the periphery. In contrast, the heat-killed Mtb cells reside in the perinuclear region (Supplementary Fig. 1a).

The analysis of spatial localization revealed an inherent cellular heterogeneity amongst live intracellular Mtb cells. Next, we examined whether heterogeneity affects intracellular bacilli's fate. Toward this, we infected THP-1 monocyte-derived macrophages with Mtb over-expressing GFP and stained the lysosomes/phagolysosomes with antibodies against the lysosomal-associated membrane protein 1 (LAMP-1). We determined the Mtb colocalization with lysosomes in perinuclear and peripheral regions. We found that perinuclear Mtb cells were more likely to be in lysosomes than peripheral ones (Fig. 1f, g). To validate the significance of these findings in tuberculosis pathogenesis, we infected mice with Mtb for two weeks, and lung tissue sections were analyzed for the subcellular distribution of Mtb and their propensity for delivery to lysosomes. This time point was chosen to avoid the overwhelming influence of adaptive immune system activation on the mycobacterial positioning. Importantly, the lung cells (100–200 μm^2) are considerably smaller than the THP-1 cells (average surface area of 400–1000 μm^2) (Supplementary Fig. 1b). To define the perinuclear region, we measured the ratio of the perinuclear region and total cell area. A 3 μm concentric ring in THP-1 cells gives an area of concentric ring/area of cell of 0.36. A similar ratio was observed with a 1 μm concentric ring in the lung tissue (Supplementary Fig. 1c). Thus, we binned the mycobacterial cells around the nucleus within increasing distance by 1 μm in the lung cells. We observed that the mycobacterial cells were distributed relatively evenly in the lung cells (Fig. 1h), and only a small fraction of mycobacterial cells (around 20%) localized with LAMP-1 marked lysosomes (Fig. 1i and Supplementary Fig. 1d). A large fraction of Mtb cells that colocalized with the lysosomes were within 1 μm from the nucleus (Fig. 1j). These findings show that Mtb resists the retrograde movement of phagosomes towards the perinuclear cloud of lysosomes, wherein the propensity of delivery to the lysosomes is higher.

https://doi.org/10.1038/s41467-025-64404-z

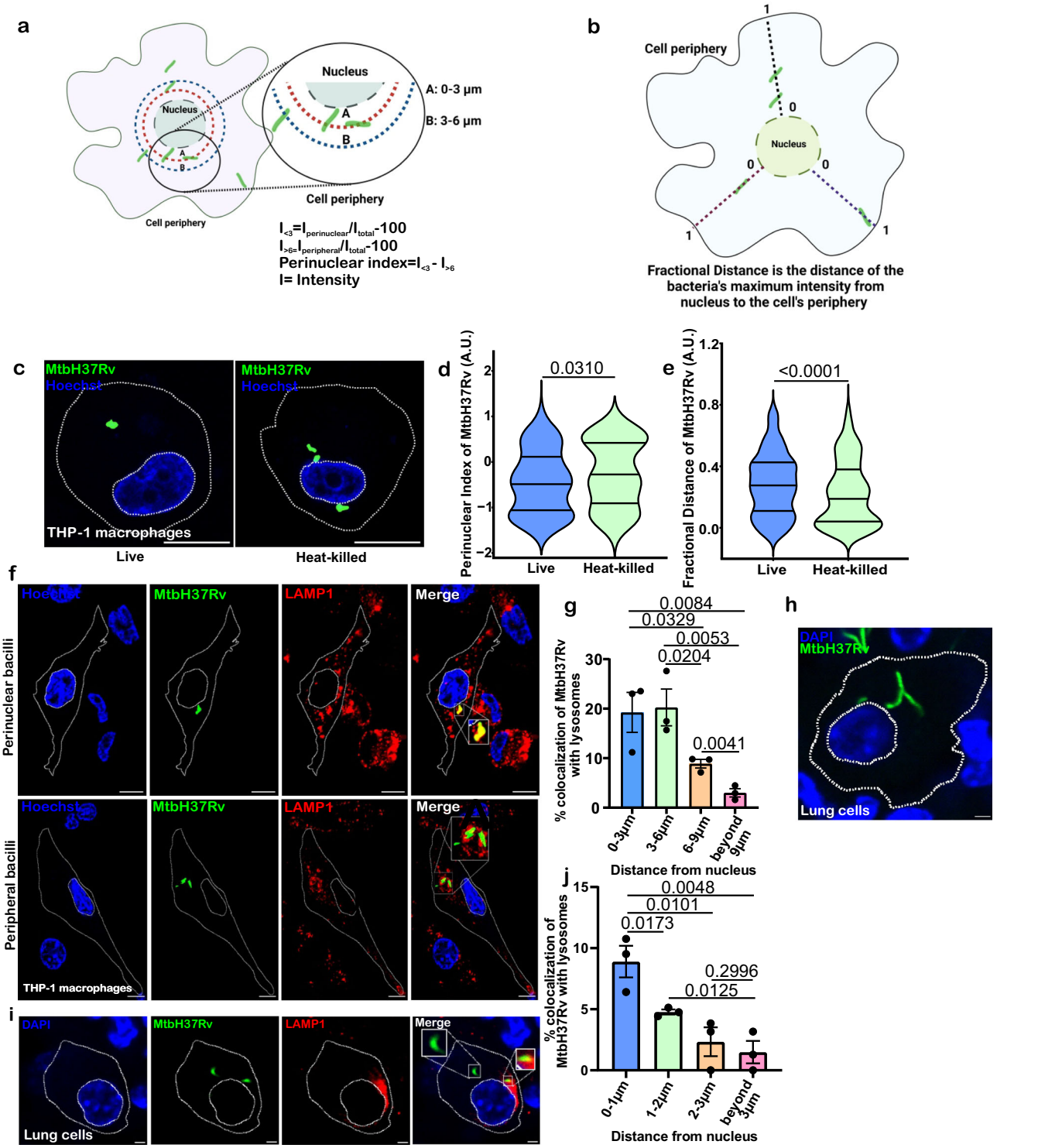

Subcellular localization of intracellular mycobacteria is tightly associated with its bioenergetics, replication rate, and drug tolerance

We recently re-engineered the ATP/ADP sensor Perceval HR (PHR)[29] into PHR-mCherry for monitoring bioenergetics of slow and fast-growing *Mycobacterium*[24]. We used Mtb overexpressing PHR-mCherry to see if Mtb's sub-cellular location relative to the nucleus affects mycobacterial bioenergetics. We infected THP-1 with Mtb over-expressing PHR-mCherry and determined the ATP/ADP levels in Mtb cells localized within concentric rings of 3, 6, 9 µm, and beyond 9 µm from the nucleus. Mtb cells in the perinuclear region have much lower ATP/ADP levels compared to those residing in the cellular periphery (Fig. 2a, b). Since Mtb's cellular bioenergetics state is tightly linked to its replication state, we also investigated whether Mtb's sub-cellular localization affects its replication. We used Mtb episomally expressing replication probe SSB-GFP, smyc'::mCherry[22], wherein GFP is fused with single-stranded binding protein (SSB) that marks the replication fork and disappears in the absence of replication[30]. Expression of SSB-GFP was normalized by mCherry. We observed that a small fraction of Mtb cells undergo DNA replication within 6 µm of the nucleus (Fig. 2c, d). In contrast, a much larger percentage of cells beyond 6 µm

https://doi.org/10.1038/s41467-025-64404-z

Fig. 1 | *M. tuberculosis* modulates its retrograde transport to the perinuclear region to avert delivery to the lysosomes. a Calculation of perinuclear index of Mtb distribution inside macrophages. Green- Mtb cells, red- 3 µm concentric ring, and blue- 6 µm concentric ring. **b** Fractional distance of Mtb distribution inside macrophages. Green—bacterial cells. **a**, **b** were created using BioRender.com. **c** THP-1 macrophages were infected with GFP-MtbH37Rv (live and heat-killed) for 3 h. The figure shows the representative images of THP-1 macrophages infected with GFP-MtbH37Rv (live and heat-killed). Violin plots depicting perinuclear index (**d**, $n = 70–75$) and fractional distance (**e**, $n > 90$) of GFP-MtbH37Rv in cells were quantified from experiments described in (**c**) (One-tailed, Mann–Whitney U test, Confidence Interval-95%). Values are represented as arbitrary units (A.U.) in violin plots. **f** THP-1 macrophages were infected with GFP-MtbH37Rv to analyze whether Mtb's spatial localization affects its delivery to lysosomes. Inset shows an enlarged region of interest containing Mtb. **g** Percent colocalization of GFP-MtbH37Rv with lysosomes (stained with anti-LAMP1) at different distances from the nucleus (stained with Hoechst dye) ($n = 110$). Data were quantified from experiments described in **f** (One-tailed, unpaired Student's *t* test, CI-95%). **h** C3HeB/FeJ mice were infected with MtbH37Rv for two weeks. The representative image shows lung cells infected with MtbH37Rv (green) and its distance from the nucleus (blue, stained with DAPI). **i** Lung sections described in h were utilized for immunostaining against LAMP-1 protein. **j** Percent colocalization of MtbH37Rv with lysosomes at different distances from the nucleus ($n = 45$) was quantified from experiments described in (**i**) (One-tailed, unpaired Student's *t* test, CI-95%). Data in **d**, **e** represent Mtb distribution in four quarters with median (central line), first quartile (upper line), and third quartile (lower line) from three independent biological experiments. Data in **g**, **j** represent mean ± SEM from three independent biological experiments. Scale Bar: 10 µm for **c**, **f** and 2 µm for **h**, **i**.

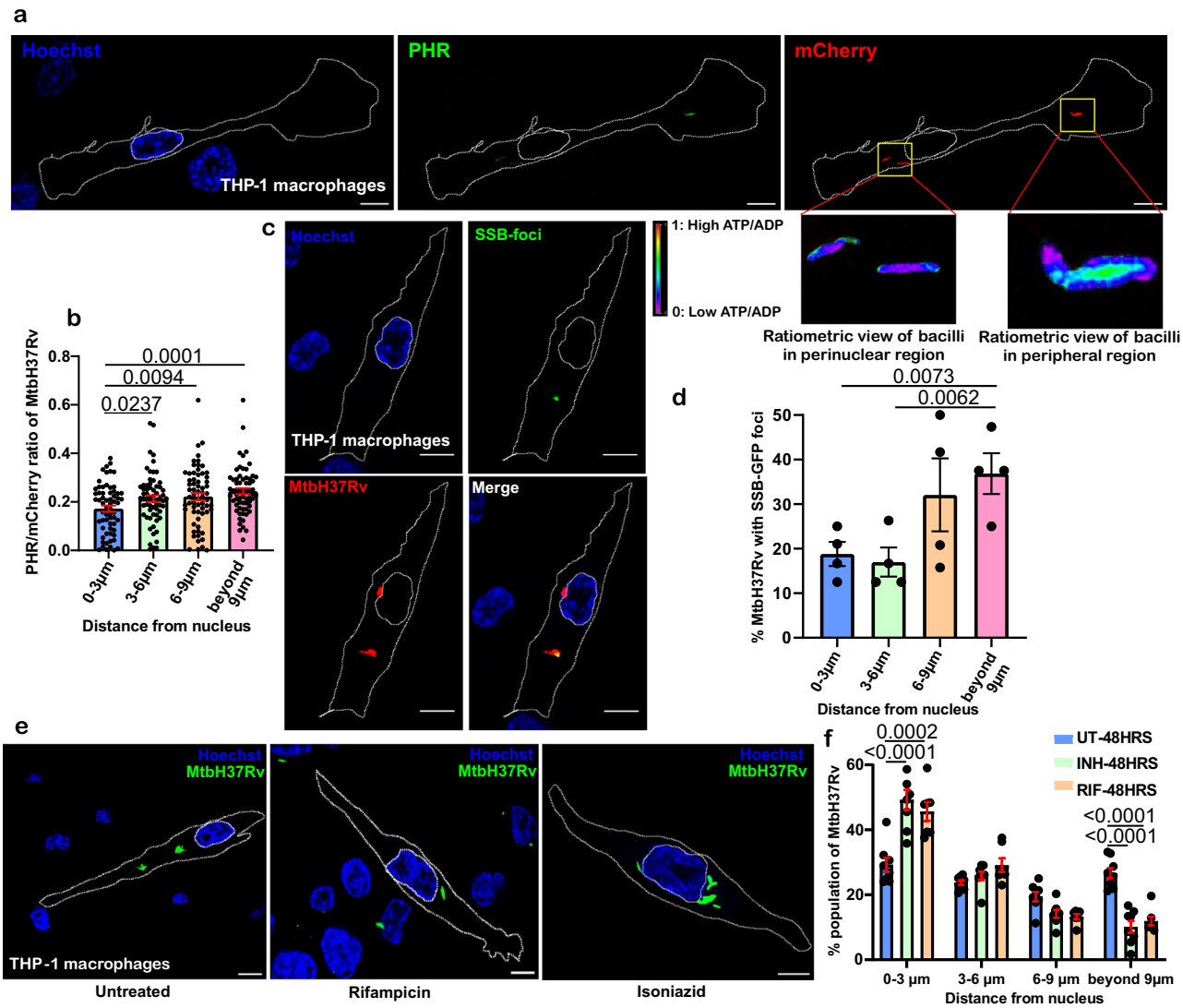

Fig. 2 | Subcellular localization of intracellular *M. tuberculosis* governs its bioenergetic state, replication rate, and response to drugs. a A representative image of THP-1 macrophages infected with Mtb-overexpressing PHR-mCherry. The inset shows the ratiometric view of perinuclear and peripheral bacilli. **b** Plot of ATP/ADP ratio of mycobacteria infecting THP-1 macrophages at different distances from the nucleus ($n = 60$) (One-tailed, Mann–Whitney U test, CI-95%). **c** THP-1 macrophages were infected with MtbH37Rv (SSB-GFP, smyc'::mCherry). The figure shows the representative image of THP-1 macrophages infected with Mtb-overexpressing SSB-GFP. **d** Percent MtbH37Rv expressing SSB-GFP ($n = 60$) foci located at different distances from the nucleus was quantified from experiments described in (**c**) (One-tailed, unpaired Student's *t* test, CI-95%). **e** THP-1 macrophages were infected with GFP-MtbH37Rv for 3 h and treated with Rifampicin or Isoniazid for 48 h post-infection. The figure shows the representative image of GFP-MtbH37Rv in untreated, Rifampicin-treated, and Isoniazid-treated macrophages. **f** Percent population of GFP-MtbH37Rv survived at different distances from the nucleus upon antibiotic treatments ($n > 200$) was quantified from experiments described in (**e**) (One-tailed, unpaired Student's *t* test, CI-95%). Data in **b**, **d**, **f** represent mean ± SEM from three independent biological experiments. Scale Bar: 10 µm.

from the nucleus had SSB-GFP puncta, indicating more replicative Mtb cells in the periphery (Fig. 2c, d).

Metabolism and replication rates are associated with the capability of Mtb to tolerate drugs[31]. Given that sub-cellular localization dictates the metabolic state and replication status of Mtb, we next analyzed if intracellular drug tolerance is associated with subcellular localization of Mtb. We infected THP-1 cells with Mtb and treated them independently with front-line anti-tuberculosis drugs, namely Isoniazid and Rifampicin, for 48 h. Subcellular localization of surviving Mtb cells was determined. Mtb cells that survive the drug treatment with either of the drugs localized primarily in the perinuclear region (Fig. 2e, f). These observations suggest that the Mtb cells in the perinuclear region are persister with lower metabolic and replication rates, while those in the peripheral region are actively replicating, have higher metabolic rates, and are susceptible to drugs.

Virulence of mycobacteria is tightly associated with its sub-cellular localization

We infected THP-1 monocyte-derived macrophages with virulent MtbH37Rv and avirulent MtbH37Ra to determine if Mtb pathogenicity is linked to phagosome subcellular mobility. We observed that avirulent MtbH37Ra localizes close to the nucleus, while virulent MtbH37Rv localizes away from the nucleus (Fig. 3a–c). A significant fraction of the avirulent Mtb population was within 3–6 μm from the nucleus. On the contrary, a substantial portion of the virulent MtbH37Rv population was away from the nucleus (Fig. 3d). Importantly, MtbH37Rv cells were studied for 12 hrs, and they were found to be in the peripheral region (Supplementary Fig. 2a, b). Since these analyses were based on images taken at one focal plane while the cell is three-dimensional, these findings were confirmed in 3-D images obtained through confocal imaging (Supplementary Fig. 3a) and transmission electron microscopy (Supplementary Fig. 3b). We also checked the subcellular localization of another virulent strain, Mtb CDC1551, and compared it with the avirulent strain MtbH37Ra. We found that Mtb CDC1551 also has peripheral localization (Supplementary Fig. 3c–e). These observations suggest that the sub-cellular localization of Mtb is tightly associated with its virulence.

Mtb sheds several lipids in macrophages[32]. Many of these lipids alter phagosome maturation[33]. Thus, Mtb could modulate the maturation of all the phagosomes. However, proteinaceous virulence factors like ESAT-6/CFP-10 are localized on cell surface[34] and thus modulate only the maturation of phagosomes harboring it. To test these possibilities, we co-infected THP-1 cells with MtbH37Rv overexpressing mCherry and MtbH37Ra overexpressing GFP. Even during coinfection, the virulent MtbH37Rv localizes away from the nucleus, while the avirulent MtbH37Ra localizes close to the nucleus (Supplementary Fig. 3f–i).

We next analyzed the sub-cellular localization of MtbΔPhoP, an attenuated deletion mutant of Mtb[35], and compared it with MtbH37Rv. We observed that MtbΔPhoP localizes close to the nucleus while the virulent MtbH37Rv localized to the cellular periphery (Fig. 3e–g). We then examined the subcellular location of MtbΔRD1, a significantly attenuated strain that lacks RD1, a 9.5 Kb genomic locus essential for mycobacterial survival in macrophages. This locus is part of Mtb's ESX-1 Type VII secretion system involved in the secretion of virulence factors ESAT-6 and CFP-10[36]. We observed that MtbΔRD1 localizes in the perinuclear region (Fig. 3h–j). The perinuclear localization of MtbΔRD1 was confirmed using a 3-dimensional confocal image rendering and electron microscopy (Supplementary Fig. 3j, k). Since PhoP regulates the secretion of ESAT-6 and CFP-10[37] and because the MtbΔRD1 is localized in the perinuclear region, we analyzed the specific role of ESAT-6 and CFP-10 in modulating the spatial localization of intracellular Mtb. Towards this, we utilized the knockout strain of Mtb (MtbΔCE) wherein specifically *CFP*-10 *(Rv*3874*)* and *ESAT*-6 *(Rv*3875*)* have been deleted[38]. Again, we observed that the MtbΔCE localizes in the perinuclear region while the parent strain localizes in the cellular periphery (Fig. 3k–m and Supplementary Fig. 3l).

Perinuclear localization of *M. tuberculosis* is critical for its delivery to lysosomes and killing

Since Mtb-laden cargo fuses with lysosomes mainly in the perinuclear region, we investigated whether decreasing retrograde transport of the avirulent MtbH37Ra reduces its killing. Toward this, we utilized knockdown of the large subunit of dynein motor (DHC) and small-molecule inhibitor Ciliobrevin D[39]. DHC knockdown resulted in disruption of perinuclear lysosomal distribution (Supplementary Fig. 4a) as reported earlier[28]. Interestingly, DHC knockdown (Fig. 4a–c) and Ciliobrevin D treatment (Supplementary Fig. 4b–d) inhibited retrograde transport of MtbH37Ra. Ciliobrevin D treatment also hampered the retrograde transport of mCherry-MtbΔRD1-laden cargoes (Supplementary Fig. 4e–g). LAMP1 staining showed that dynein subunit knockdown inhibits delivery of MtbH37Ra to the lysosomes (Fig. 4d, e). We then examined how dynein's large subunit knockdown affected MtbH37Ra intracellular survival in macrophages. We found that dynein knockdown significantly reduces MtbH37Ra killing inside macrophages (Fig. 4f).

We hypothesized that genetically induced perinuclear localization of phagosomes containing virulent Mtb could enhance mycobacterial delivery to lysosomes and reduce intracellular mycobacterial survival. We utilized knockdown of ADP-ribosylation factor like protein 8B (ARL8B). ARL8B plays an important role in the anterograde transport of lysosomes by recruiting SifA and kinesin interacting protein and kinesin 1[40,41]. Its knockdown is known to induce perinuclear clustering of lysosomes[41]. ARL8B ablation was confirmed through western blot analysis (Supplementary Fig. 5a). ARL8B ablation leads to perinuclear localization of Mtb (Fig. 4g–i) and increased delivery to lysosomes (Fig. 4j, k). ARL8B ablation significantly killed virulent Mtb (Fig. 4l). These results were verified using a knockdown of ARL8A (Supplementary Fig. 5b–h), which is functionally similar to ARL8B[42]. We also observed that ARL8B ablation in macrophages does not improve the killing of avirulent MtbH37Ra (Supplementary Fig. 5i). In conclusion, Mtb killing depends on the perinuclear localization of Mtb-laden phagosomes.

IFN-γ induces perinuclear localization of lysosomes

IFN-γ activates naïve macrophages[43,44] leading to maturation and acidification of the phagosome[45], induction of autophagy flux[2], and lysosomal proteases[46]. However, its effect on lysosomal positioning is unknown. To examine the effect of IFN-γ on lysosome positioning, we treated bone marrow-derived macrophages (BMDMs) with IFN-γ for 3 h and analyzed lysosomal positioning using immunostaining of LAMP1. We observed that treatment with IFN-γ results in juxtanuclear clustering of lysosomes (Supplementary Fig. 6a–c). These observations were confirmed in the THP-1-derived macrophages (Supplementary Fig. 6d–f). We performed live-cell imaging to determine the kinetics of IFN-γ-induced perinuclear clustering of lysosomes. IFN-γ treatment induces lysosome clustering in the juxtanuclear area within 15 min (910 s panel) (Supplementary Fig. 6g and Supplementary Video 1a, b). IFN-γ treatment increases lysosome size (Supplementary Fig. 6h) concomitant to their movement toward the nucleus but does not modulate their speed or displacement rate (Supplementary Fig. 6i, j). Activation of phagocytosis is known to result in an expansion of lysosomal volume[47]. It is well known that lysosomes have a variable pH. Thus, we analyzed the acidification of lysosomes vis-à-vis their perinuclear localization upon treatment with IFN-γ. We labeled the lysosomes overnight with Dextran coupled to Alexa Fluor 647, a pH-insensitive far-red emitting fluorophore as described previously[26]. After that, cells were exposed to LysoTracker Green, a dye that accumulates in acidic organelles. We observed that IFN-γ treatment

https://doi.org/10.1038/s41467-025-64404-z

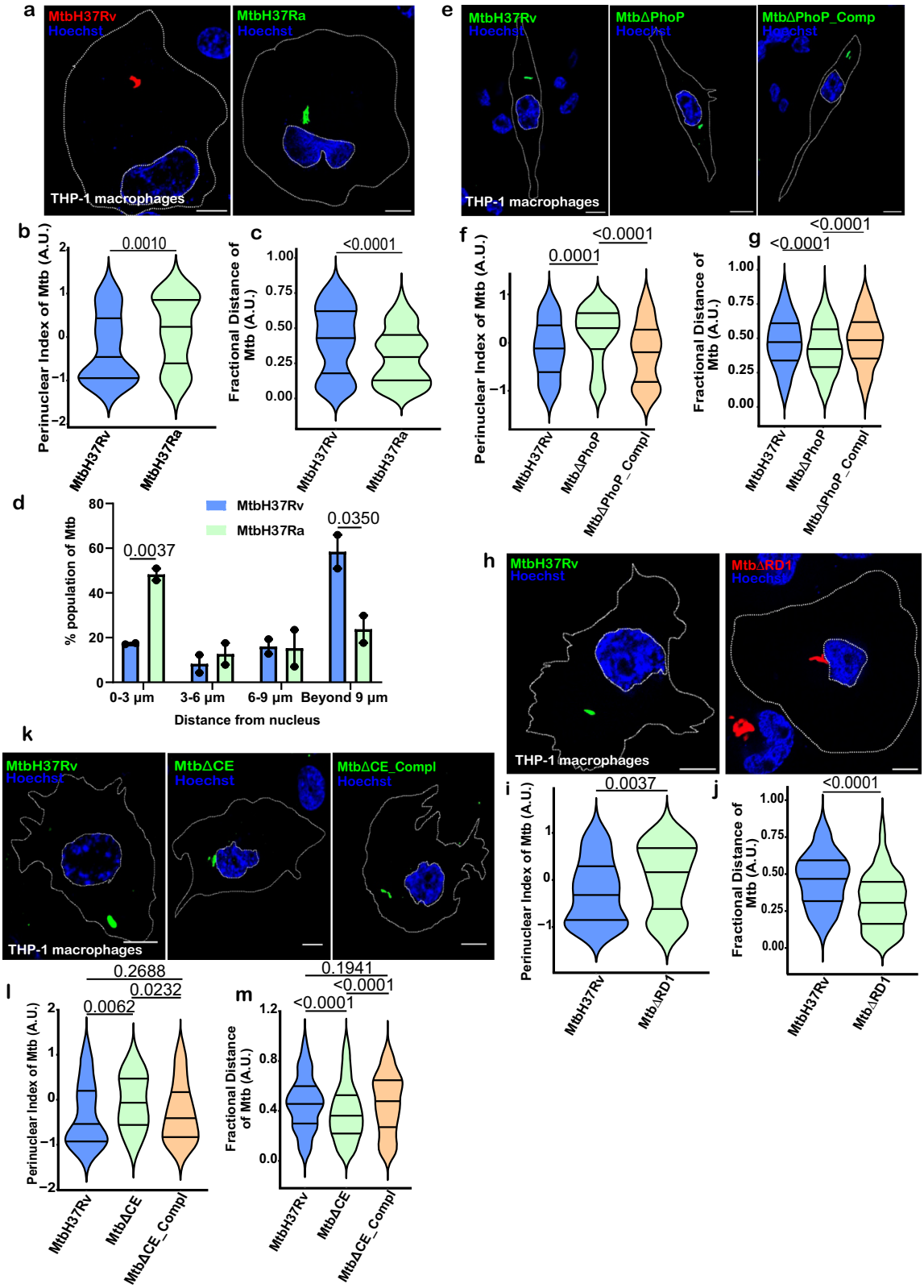

mediated perinuclear localization of lysosomes is also associated with their acidification (Supplementary Fig. 6k–m).

IFN-γ induces perinuclear positioning of virulent mycobacteria and its delivery to lysosomes

IFN-γ can alleviate Mtb-mediated suppression of the phagosome-lysosome fusion[48]. Next, we examined if IFN-γ affects the cellular positioning of Mtb. Treatment of THP-1 macrophages with IFN-γ results in the perinuclear localization of Mtb (Fig. 5a–c). We evaluated the relative location of Mtb and found that IFN-γ promotes Mtb's clustering within 3 µm from the nucleus (Fig. 5d). Mouse BMDMs similarly showed IFN-γ-mediated perinuclear clustering of Mtb (Supplementary Fig. 7a–c). IFN-γ induces perinuclear clustering of the lysosomes and Mtb-laden cargoes, which may enhance their fusion. To

Fig. 3 | Virulence of *M. tuberculosis* is tightly associated with its subcellular localization. a THP-1 macrophages were infected with mCherry-MtbH37Rv and GFP-MtbH37Ra for 3 h. Violin plots depicting the distribution of mCherry-MtbH37Rv and GFP-MtbH37Ra in cells as perinuclear index (**b**, $n = 88–91$) and fractional distance (**c**, $n > 90$) (One-tailed, Mann–Whitney U test, CI-95%). **d** The percent population of mCherry-MtbH37Rv and GFP-MtbH37Ra in infected macrophage cells ($n = 43–55$) at different distances from the nucleus was quantified from experiments described in (**a**) (One-tailed, unpaired Student's *t* test, CI-95%). **e** THP-1 macrophages were infected with MtbH37Rv, MtbΔPhoP and complementary strain and proceeded similarly as in (**a**). Mtb cells were stained with anti-Mtb antibody, and the nucleus was counterstained with Hoechst dye. Violin plot for the distribution of MtbH37Rv, MtbΔPhoP and complementary strain in macrophage cells as perinuclear index (**f**, $n > 90$) and fractional distance (**g**, $n > 90$) (One-tailed, Mann–Whitney U test, CI-95%). **h** THP-1 macrophages were infected with GFP-MtbH37Rv and mCherry-MtbΔRD1. Violin plots depicting the distribution of GFP-MtbH37Rv and mCherry-MtbΔRD1 in macrophages and visualized as perinuclear index (**i**, $n > 80$) and fractional distance (**j**, $n > 90$) (One-tailed, Mann–Whitney U test, CI-95%). **k** THP-1 macrophages were infected with MtbH37Rv, MtbΔCE, and complementary strain (1:10 MOI) and proceeded similarly as in (**e**). Violin plots depicting the distribution of MtbH37Rv, MtbΔCE, and complementary strain in macrophage cells as perinuclear index (**l**, $n > 55$) and fractional distance (**m**, $n > 90$) (One-tailed, Mann–Whitney U test, CI-95%). Data in **b**, **c**, **f**, **g**, **i**, **j**, **l**, **m** represent Mtb distribution in four quarters (with median (central line), first quartile (upper line), and third quartile (lower line) from three independent biological experiments. Data in **d** represents mean ± SEM from two independent biological experiments. Scale Bar: 10 µm.

examine this, we infected THP-1 macrophages with GFP-MtbH37Rv and stained lysosomes with LAMP1. As expected, IFN-γ promotes the delivery of MtbH37Rv into lysosomes in the perinuclear area (Fig. 5e, f). The majority of Mtb-lysosome colocalization takes place within 0–3 µm from the nucleus. Importantly, even in the control macrophages, Mtb colocalizes with lysosomes, primarily in the perinuclear area (Fig. 5e, f). Next, we examined if inhibiting Mtb's perinuclear location affects IFN-γ-mediated MtbH37Rv killing. Knocking down dynein inhibits IFN-γ-mediated perinuclear localization of Mtb (Fig. 5g–i) and delivery to lysosomes (Fig. 5j, k). The ablation of dynein function by siRNA or Ciliobrevin D inhibits IFN-γ mediated killing of intracellular Mtb cells (Fig. 5l, m). Given that RAB7 facilitates the recruitment of RILP, which is an adapter of tethering lysosomes onto dynein motor, next we analyzed the role of RILP in IFN-γ mediated perinuclear localization of Mtb. Towards this, we used siRNA-based knockdown of RILP. We observed that RILP knockdown does not affect the IFN-γ-mediated perinuclear localization of Mtb (Supplementary Fig. 8a–d). These observations suggest that a non-canonical signaling axis may work in the IFN-γ-mediated perinuclear localization of Mtb.

TFEB regulates IFN-γ mediated retrograde transport of mycobacteria through enhanced expression and interaction of TMEM55B and JIP4

We have earlier demonstrated that IFN-γ induces nuclear translocation of TFEB, which modulates the fusion of phagosomes and autophagosomes with lysosomes to restrict intracellular mycobacterial growth[49]. We used TFEB knockdown to investigate if TFEB affects Mtb's centripetal movement and intracellular Mtb survival in response to IFN-γ. We found that TFEB ablation (confirmed using western blot analysis, Fig. 6f) inhibits IFN-γ-induced migration of MtbH37Rv toward the nucleus (Fig. 6a–c). Colony-forming unit (CFU) analysis suggested that TFEB is critical for IFN-γ-mediated mycobacterial killing (Fig. 6d). Recently, TFEB was shown to upregulate TMEM55B (also known as PIP4P1), which recruits the dynein adapter JIP4 to the lysosome. JIP4 then recruits the dynein-dynactin motor complex to transport lysosomes toward the microtubules at minus-end[50]. Considering these findings, we investigated if IFN-γ-induced macrophage activation results in *TMEM55B* upregulation. IFN-γ treatment leads to TFEB-dependent upregulation of *TMEM55B* mRNA and TMEM55B protein in THP-1 macrophages, as shown by qRT-PCR and western blot analysis (Fig. 6e, f). Since the *JIP4* promoter also harbors the coordinated lysosomal expression and regulation motif[51] (Supplementary Fig. 9a), we also analyzed the expression of *JIP4* in IFN-γ-treated THP-1 macrophages. Similar to *TMEM55B*, we observed that *JIP4* expression is induced upon IFN-γ treatment (Fig. 6g). To confirm this, we also performed ChIP PCR with DNA enriched through TFEB antibodies and found that TFEB binds to the *JIP4* promoter upon treatment with IFN-γ (Fig. 6h and Supplementary Fig. 9b). We used lysosome enrichment and immunoprecipitation to investigate if IFN-γ enhances JIP4 and TMEM55B levels and their interaction on lysosomes. Upon treatment with IFN-γ, JIP4, and TMEM55B levels increased on lysosomes (Fig. 6i), and their interaction was greatly enhanced (Fig. 6j).

TFEB-TMEM55B-JIP4 axis drives retrograde lysosomal trafficking mediated by IFN-γ

Up-regulation of expression of TMEM55B could modulate the spatial localization of Mtb-laden cargoes, through their interaction with dynein adapter JIP4. Thus, next, we analyzed the role of TMEM55B in IFN-γ-mediated delivery of Mtb to the perinuclear space and lysosomes. We knocked down TMEM55B (confirmed through western blot analysis, Supplementary Fig. 9c). TMEM55B knockdown resulted in attenuation of IFN-γ-mediated retrograde transport of virulent MtbH37Rv (Fig. 7a–c) and their delivery to lysosomes (Fig. 7d, e). This also reduces the killing of intracellular MtbH37Rv in response to IFN-γ (Fig. 7f). Next, we analyzed whether the expression of dynein adapter JIP4 is critical in IFN-γ-induced perinuclear positioning of Mtb. We used siRNA-based knockdown to confirm the role of JIP4 in the retrograde trafficking of MtbH37Rv via IFN-γ (confirmed through western blot analysis, Supplementary Fig. 9d). JIP4 knockdown reduced IFN-γ-mediated centripetal movement of MtbH37Rv (Fig. 7g–i). JIP4 knockdown also resulted in reduced colocalization of MtbH37Rv with LAMP1 (Fig. 7j, k) and reduced IFN-γ-mediated killing of intracellular MtbH37Rv (Fig. 7l). These observations suggest that the recruitment of TMEM55B onto Mtb-laden cargoes enables their loading onto dynein motors through JIP4. This leads to the centripetal movement of Mtb and its delivery to lysosomes, wherein Mtb is killed.

Discussion

After infecting macrophages, Mtb cells are distributed in phagosomes, autophagosomes, phagolysosomes, and cytoplasm. However, their spatial localization and its relevance to the infection have remained unclear. Here, we have demonstrated that pathogenic MtbH37Rv and Mtb CDC1551 localize in the cellular periphery while avirulent H37Ra and virulence gene deletion-mediated attenuated MtbH37Rv strains are transported to perinuclear cloud where they are delivered to the lysosomes. This spatial distribution and delivery to lysosomes is also observed in lungs during mice aerosol infection. Importantly, Mtb cells in the perinuclear region are metabolically quiescent, non-replicating, and display drug tolerance, while those in the peripheral region are metabolically active, replicating, and drug-responsive. Furthermore, we demonstrated that IFN-γ activation in macrophages leads to retrograde transport of virulent MtbH37Rv to the juxtanuclear region, where MtbH37Rv cells are killed, whereas inhibiting this transport affects the IFN-γ-mediated killing of MtbH37Rv. In agreement with these findings, we discovered that ARL8B silencing promoted retrograde trafficking of lysosomes and Mtb-laden cargoes, boosting MtbH37Rv's perinuclear localization and killing. Earlier, the Rab7-RILP axis has been shown to transport the phagosome towards the nucleus[52]. Here, we have defined the TFEB-regulated TMEM55B-JIP4 axis that plays a critical role in IFN-γ-mediated retrograde trafficking of lysosomes and MtbH37Rv. The findings of this study are summarized

https://doi.org/10.1038/s41467-025-64404-z

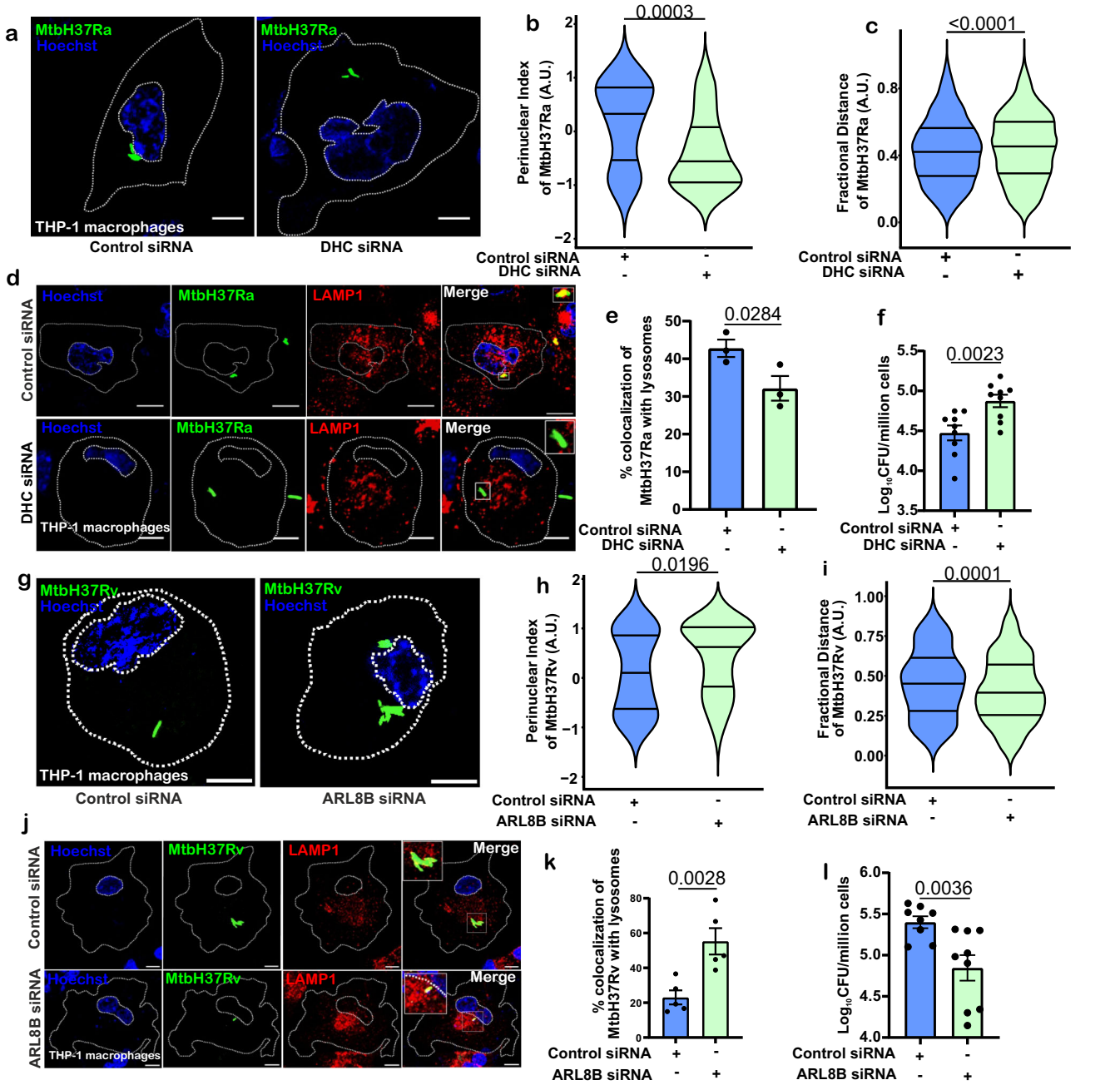

Fig. 4 | Perinuclear localization of *M. tuberculosis*-laden cargo is critical its delivery to lysosomes and killing. a THP-1 macrophages were treated with control siRNA and Dynein heavy chain (DHC) siRNA for 48 h and infected with GFP-MtbH37Ra for 3 h. Violin plots depicting the distribution of GFP-MtbH37Ra in macrophage cells as perinuclear index (**b**, $n = 69$) and fractional distance (**c**, $n > 90$) (One-tailed, Mann–Whitney U test, CI-95%). **d** THP-1 macrophages were treated with control and DHC siRNA followed by infection with GFP-MtbH37Ra. Cells were stained with anti-LAMP1 antibody for visualizing lysosomes. The inset shows an enlarged region of interest for examining Mtb's delivery to lysosomes. **e** The graph depicts the percent colocalization of GFP-MtbH37Ra with lysosomes (stained with anti-LAMP1 antibody) ($n = 48–51$) (One-tailed, unpaired Student's *t* test, CI-95%). **f** MtbH37Ra survival in THP-1 macrophages treated with control siRNA or DHC siRNA was calculated through CFU estimation (One-tailed, unpaired Student's *t* test, CI-95%). **g** THP-1 macrophages were treated with control and ARL8B siRNA, followed by infection with GFP-MtbH37Rv for 3 h. Violin plots depicting the distribution of GFP-MtbH37Rv in macrophage cells as perinuclear index (**h**, $n > 60$) and fractional distance (**i**, $n > 90$) (One-tailed, Mann–Whitney U test, CI-95%). **j** THP-1 macrophages were treated with control siRNA or ARL8B siRNA and infected with GFP-MtbH37Rv. Cells were stained for lysosomes with anti-LAMP1 antibody. The inset shows an enlarged region of interest for examining Mtb's delivery to lysosomes. **k** The graph depicts the percent colocalization of GFP-MtbH37Rv with lysosomes (stained with anti-LAMP1 antibody) ($n = 55$) were quantified from experiments described in (**j**) (One-tailed, unpaired Student's *t* test, CI-95%). **l** MtbH37Rv survival in THP-1 macrophages treated with control siRNA or ARL8B siRNA post-infection was calculated through CFU estimation (One-tailed, unpaired Student's *t* test, CI-95%). Data in **b**, **c**, **h**, **i** represent Mtb distribution in four quarters (with median (central line), first quartile (upper line), and third quartile (lower line) from three independent biological experiments. Data in **e**, **f**, **k**, **l** are represented in mean ± SEM from three independent biological experiments. Scale Bar: 10 μm.

https://doi.org/10.1038/s41467-025-64404-z

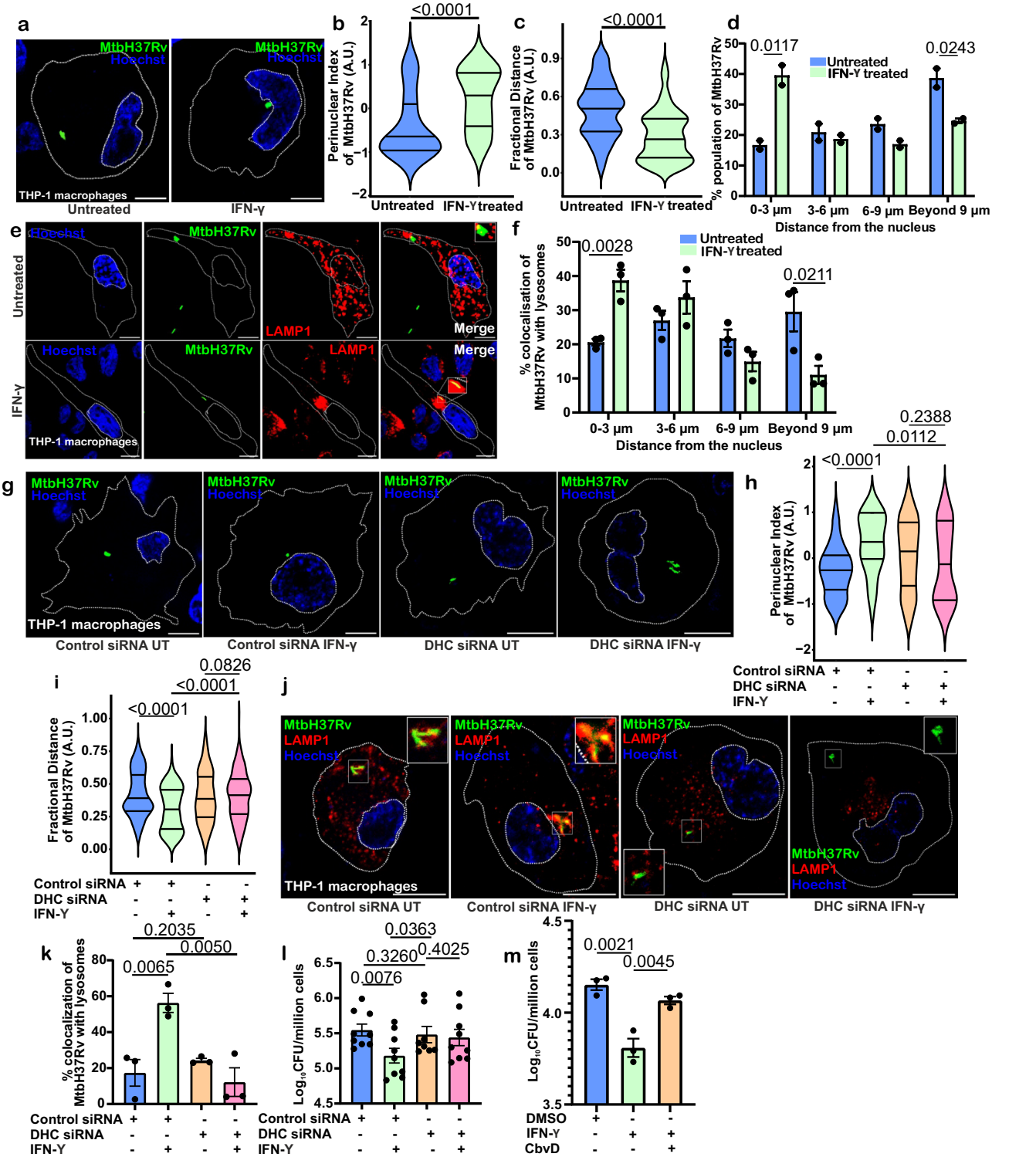

in Fig. 8, which provides a working model for the current spatial understanding of Mtb inside the macrophages.

This study revealed that only a few of the virulent Mtb cells are delivered to the perinuclear region upon phagocytosis, while the majority of the virulent Mtb cells can resist such perinuclear localization. This kind of heterogeneity in spatial distribution was not known earlier. Earlier, Mtb's metabolism[24] and redox homeostasis[21] heterogeneity were linked to drug tolerance of Mtb in different subcellular compartments, such as phagosomes and phagolysosomes, etc. We have shown that the differences in spatial localization led to marked heterogeneity of intracellular Mtb in terms of metabolism, replication, intracellular survival, and susceptibility/resistance to drugs. These observations provide another dimension towards explaining the enhanced drug tolerance observed inside the macrophages. Earlier, the heterogeneity of mycobacterial cells during infection in animal tissue was appreciated. Such heterogeneity arose from different microenvironment perceived by Mtb in different regions and types of granulomas inside animal[15,53–56]. This heterogeneity was ascribed as one of the reasons for the requirement of prolonged treatment for tuberculosis. The factors that regulate such heterogeneity remain unknown. In this study, we have described the inherent heterogeneity in the intracellular mycobacteria arising from differential spatial localization.

Fig. 5 | IFN-γ induces perinuclear positioning of *M. tuberculosis* and its delivery to lysosomes. a THP-1 macrophages were infected with GFP-MtbH37Rv and stimulated with IFN-γ for 3 h. Violin plots depicting the distribution of GFP-MtbH37Rv in macrophage cells as perinuclear index (**b**, $n = 52$) and fractional distance (**c**, $n > 90$) (One-tailed, Mann–Whitney U test, CI-95%). **d** Percent population of GFP-MtbH37Rv in THP-1 macrophages treated with or without IFN-γ at different distances from the nucleus ($n = 60$) (One-tailed, unpaired Student's t test, CI-95%). **e** THP-1 macrophages were infected with GFP-MtbH37Rv and stimulated with IFN-γ and stained with anti-LAMP1 antibody for marking lysosomes. The inset shows an enlarged region of interest for examining Mtb's delivery to lysosomes. **f** Percent colocalization of GFP-MtbH37Rv with lysosomes (stained with anti-LAMP1) at different distances from the nucleus (stained with Hoechst dye) ($n = 63–75$) (One-tailed, unpaired Student's t test, CI-95%). **g** THP-1 macrophages were treated with control siRNA or DHC siRNA and infected with GFP-MtbH37Rv. Cells were treated with or without IFN-γ. Violin plots depicting the distribution of GFP-MtbH37Rv in macrophage cells as perinuclear index (**h**, $n = 32–40$) and fractional distance (**i**, $n > 90$) (One-tailed, Mann–Whitney U test, CI-95%). **j** THP-1 macrophages were treated with control siRNA or DHC siRNA, infected with GFP-MtbH37Rv and stimulated with IFN-γ and stained with anti-LAMP1 antibody. The inset shows an enlarged region of interest for examining Mtb's delivery to lysosomes. **k** Percent colocalization of GFP-MtbH37Rv with lysosomes (stained with anti-LAMP1 antibody) ($n = 64–85$) (One-tailed, unpaired Student's t test, CI-95%). **l** MtbH37Rv survival in THP-1 macrophages treated with control siRNA or DHC siRNA and stimulated with or without IFN-γ post-infection was calculated through CFU estimation (One-tailed, unpaired Student's t test, CI-95%). **m** Cells were pre-treated with Ciliobrevin D (20 μM/ml for 2 h) and infected with MtbH37Rv. Mycobacterial survival was calculated through CFU estimation (One-tailed, unpaired Student's t test, CI-95%). Data in **b**, **c**, **h**, **i** represent Mtb distribution in four quarters (with median (central line), first quartile (upper line), and third quartile (lower line) from three independent biological experiments. Data in **d** represent mean ± SEM from two independent biological experiments. Data in **f**, **k**, **l**, **m** represent mean ± SEM from three independent biological experiments. Scale Bar: 10 μm.

This heterogeneity may represent a betting hedge strategy used by Mtb to ensure a successful and prolonged infection. The observation that perinuclear Mtb cells are likely to be delivered to lysosomes, which can kill intracellular Mtb, is interesting and can lead to the development of new small molecules that could selectively alter the host trafficking to facilitate the perinuclear localization of Mtb and its killing for the amelioration of tuberculosis.

We further demonstrated that Mtb's subcellular position is largely governed by its virulence. Confocal microscopy and TEM analysis suggested that heat-killed, avirulent, and attenuated Mtb strains cannot impede their retrograde transport, while live virulent Mtb strains restrict their retrograde movement. Earlier studies have suggested several virulence factors secreted by MtbH37Rv that modulate phagosome maturation, such as mycobacterial protein tyrosine phosphatase A, PtpA[57], serine-threonine kinase protein kinase G (PknG)[58,59], etc. However, whether these mycobacterial factors modulate spatial positioning was not known. We used a series of experiments utilizing avirulent strain MtbH37Ra and gene deletion attenuated strains, namely, MtbΔPhoP, MtbΔRD1, and MtbΔCE, to delineate an important role of secretory virulence factors ESAT-6 and CFP-10 and Region of difference 1 (RD 1) encoded type VII secretion system to define the role of these virulence factors in subcellular positioning of MtbH37Rv. These experiments suggest that virulence factors ESAT-6 and CFP-10 secreted by RD1, encoded type VII secretion system regulated by PhoP, play a critical role in the inhibition of retrograde transport of Mtb. ESAT-6 and CFP-10 are known to form a tight heterodimer[60], which could dissociate at acidic pH[61]. At acidic pH, ESAT-6 can form a homotetramer capable of interacting with cell membranes[61]. However, which host factors are specifically modulated by ESAT-6 and CFP-10 heterodimer and ESAT-6 tetramer remain to be ascertained and is beyond the scope of this study. Further studies are required to decipher the exact molecular mechanism behind the ESAT-6 and CFP-10-mediated inhibition of retrograde transport of Mtb-laden cargoes. These studies could include the proteome analysis of MtbH37Ra-laden and MtbH37Rv-laden cargoes. Findings described in this study support an earlier study suggesting that a highly virulent strain of Mtb Beijing alters lysosomal positioning to avoid starvation-induced autophagy-mediated growth restriction[62]. The positioning of cargo containing Mtb could be influenced by loading the Mtb-laden cargoes onto dynein or the kinesin motors. We suggest that Mtb may inhibit the association of the Mtb-laden cargo with the dynein motor and prefer its interaction with the kinesin motor and these events are governed by factors associated with Mtb's virulence, including ESAT-6 and CFP-10. Earlier investigations suggest that *Salmonella enterica* serovar Typhimurium recruits the kinesin motor[63–66] to push vacuoles harboring it to the cell periphery. This recruitment of Salmonella-containing vacuole towards the MTOC in the perinuclear region is critical for the growth of Salmonella[67–69]. On the contrary, we found that virulent MtbH37Rv actively inhibits phagosome loading onto the dynein-dynactin motor to impede retrograde transport. Various pathogens also prevent fusion with the lysosomes and block the centripetal movement of pathogen-loaded phagosomes, boosting their survival[70].

Currently, the Rab7-RILP axis is known to derive the retrograde movement of the phagosome[71]. However, mycobacterial cells are known to inhibit the Rab7 recruitment[72] and its activation[52] on the phagosomes. Furthermore, we observed that IFN-γ-mediated activation does not utilize the Rab7-RILP axis for perinuclear localization and clearance of Mtb. We demonstrated that the TMEM55B-JIP4 axis is essential in the IFN-γ-induced retrograde transport of Mtb-laden phagosomes. However, the role of this pathway in the retrograde transport of other intracellular pathogens and their killing remains to be analyzed. Furthermore, it remains unknown which adapter proteins facilitate the recruitment of MtbH37Ra-laden phagosomes onto the Dynein-dynactin motors. Identifying such adapters and MtbH37Rv effectors that disrupt such recruitment will be a major milestone in the field.

Methods

Animal ethics statement

The experiments with mice were approved by the Institutional Animal Ethics Committee of Council of Scientific and Industrial Research-Institute of Microbial Technology (Approval no IAEC/19/07) or Institutional Animal Ethics Committee of Council of National Center for Biological Sciences, Bangalore (Approval no NCBS-IAE-2020/12/(R1)). These experiments were performed according to the Guidelines issued by the Committee for the Purpose of Supervision of Experiments on Animals (No.55/1999/CPCSEA) under the Prevention of Cruelty to Animals Act 1960 and amendments introduced in 1982 by the Ministry of Environment and Forest, Govt. of India. Animal infections and subsequent studies were performed at the Animal BSL-3 facility of NCBS, Bangalore.

Antibodies, chemicals, and siRNA. All the antibodies and chemicals used in the study are listed in Supplementary Tables 1, 2, and 3, respectively.

Bacterial strain and growth conditions

MtbH37Rv (ATCC, 27294), GFP-MtbH37Rv, mCherry-MtbH37Rv, MtbH37Ra (ATCC, 25177), GFP-MtbH37Ra, MtbΔRD1 (a kind gift of Dr. David Sherman), mCherry-MtbΔRD1, MtbΔCE and MtbΔCE Complementary[38] *phoPR* disruption mutant (MtbΔPhoP) and MtbΔPhoP_Complementary strain of *M. tuberculosis* H37Rv (*phoPR*-KO and complemented strain, a kind gift of Dr. Issar Smith)[35], MtbH37Rv integrated with roGFP2 (kind gift of Dr. Amit Singh), ATP/ADP reporter

https://doi.org/10.1038/s41467-025-64404-z

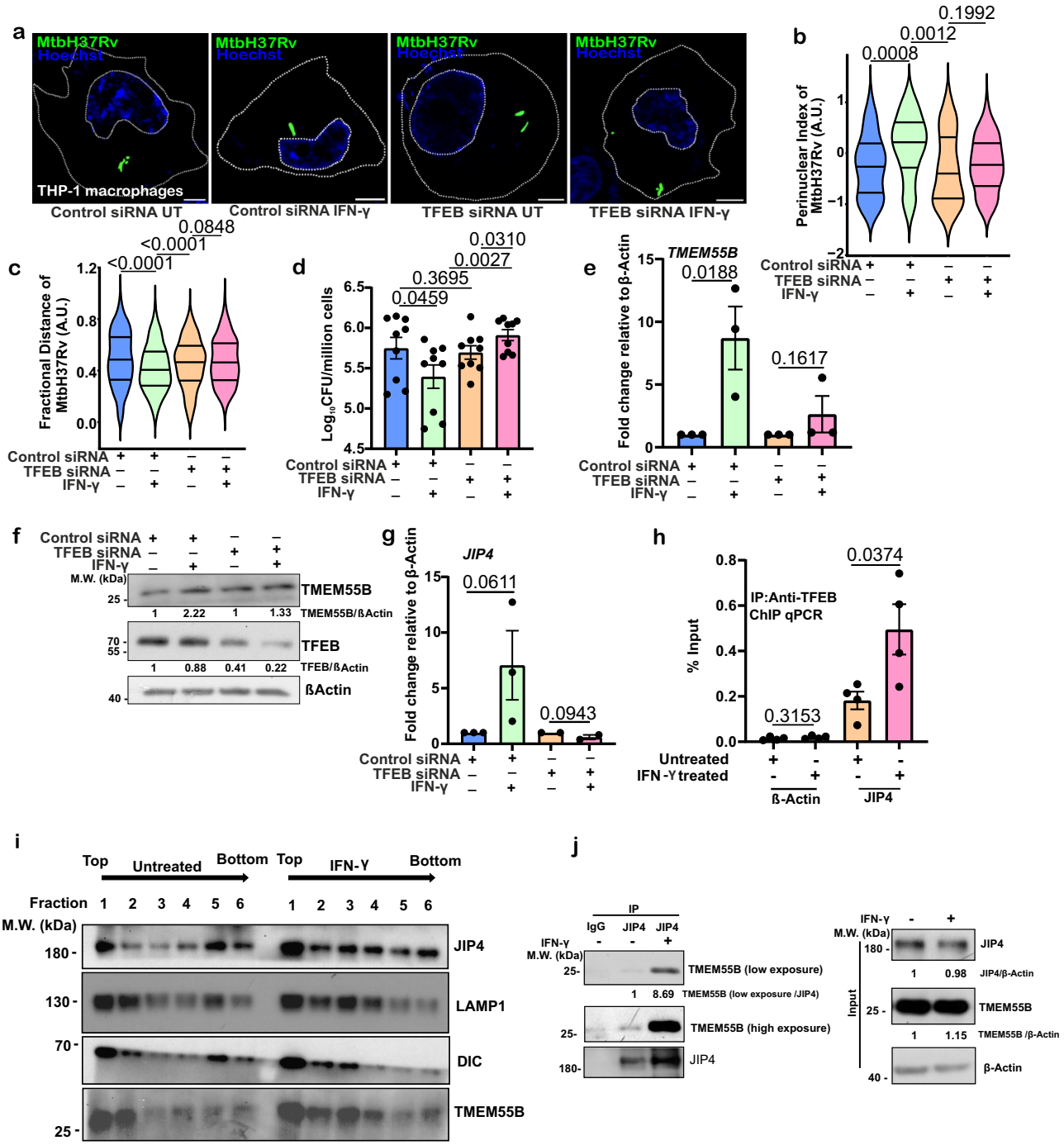

Fig. 6 | TFEB regulates IFN-γ mediated retrograde transport of *M. tuberculosis* through enhanced expression and interaction of TMEM55B and JIP4. **a** Representative Images depicting the spatial positioning of Mtb in THP-1 macrophages stimulated with IFN-γ and treated with control or TFEB siRNA. Violin plots depicting the distribution of GFP-MtbH37Rv as the perinuclear index (**b**, *n*-50) and fractional distance (**c**, $n > 60$) (One-tailed, Mann–Whitney U test, CI-95%). **d** MtbH37Rv survival computed through CFU analysis in THP-1 macrophages treated with control siRNA or TFEB siRNA and stimulated with or without IFN-γ post-infection (One-tailed, unpaired Student's *t* test, CI-95%). **e** Total RNA was isolated from cells treated with Control siRNA or TFEB siRNA (48 h) stimulated with or without IFN-γ and subjected to qRT-PCR. The graph depicts *TMEM55B* RNA-fold change (relative to β actin) (One-tailed, unpaired Student's *t* test, CI-95%). **f** Immunoblotting was performed to measure TMEM55B level in Control siRNA or TFEB siRNA-treated cells (48 h) stimulated with or without IFN-γ. The numbers below indicate the fold change of TMEM55B and TFEB relative to β actin. **g** RNA was isolated from cells treated with control siRNA or TFEB siRNA (48 h) stimulated with or without IFN-γ and subjected to qRT-PCR. The graph depicts *JIP4* RNA-fold change (relative to β actin) (One-tailed, unpaired Student's *t* test, CI-95%). **h** THP-1 macrophages were stimulated with or without IFN-γ for 3 h. ChIP assay was performed to analyze the binding of TFEB to the promoter region of *JIP4*. β actin was used as an internal control (One-tailed, unpaired Student's *t* test, CI-95%). **i** Lysosome enrichment was performed on cells treated with or without IFN-γ. Fractions 1–6 from untreated and IFN-γ treated cells were immunoblotted. **j** Lysates of THP-1 macrophages treated with or without IFN-γ were subjected to endogenous immunoprecipitation using JIP4 antibody, and the precipitates were immunoblotted with the indicated antibodies. The number below indicates the fold change of TMEM55B relative to the IP: JIP4 signal. Data in **b**, **c** represents Mtb distribution in four quarters (with median (central line), first quartile (upper line), and third quartile (lower line) from three independent biological experiments. Data in **d**, **e**, **g**, **h** represent mean ± SEM from three independent biological experiments. Scale Bar: 10 μm.

https://doi.org/10.1038/s41467-025-64404-z

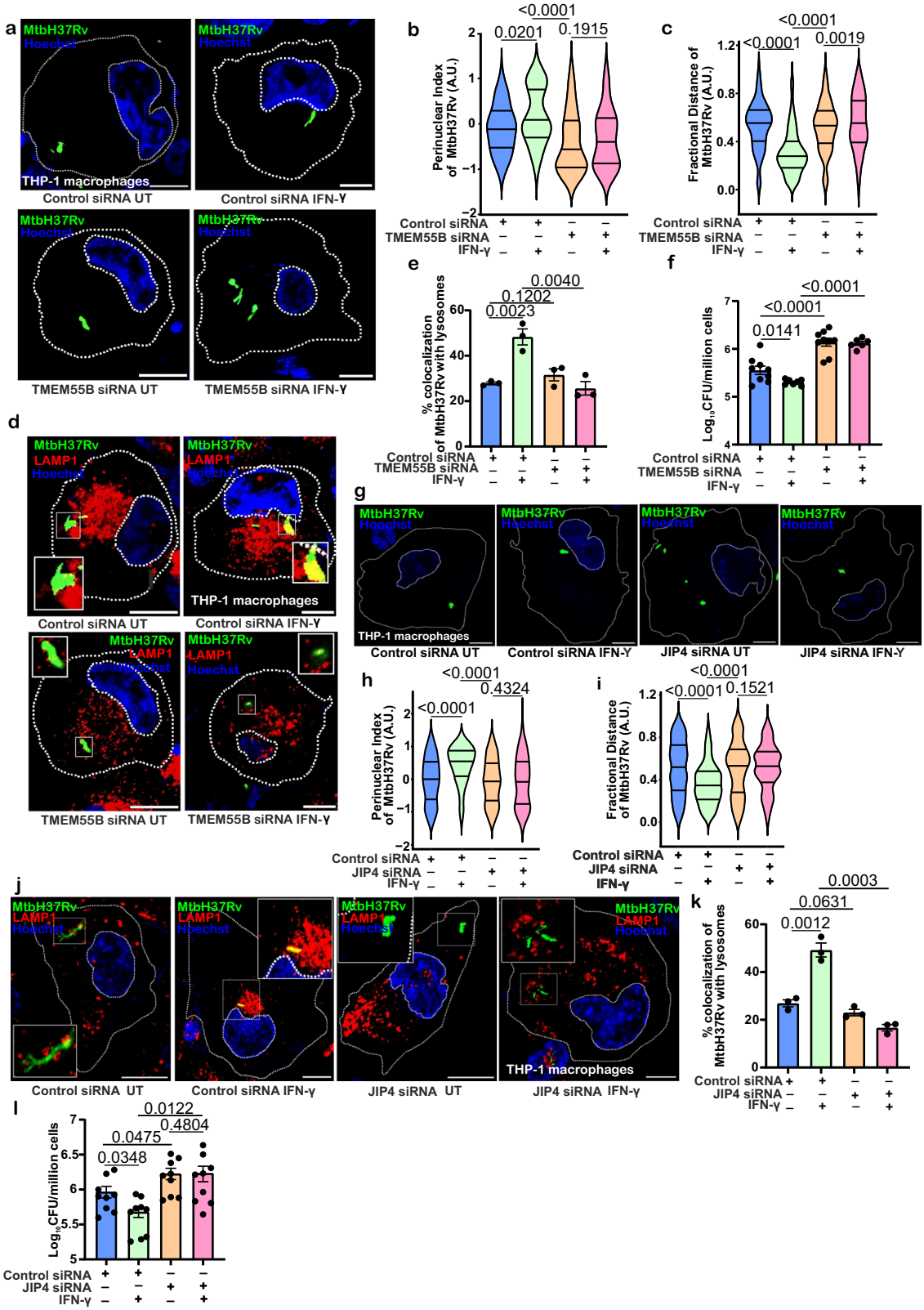

strain of Mtb expressing the PHR-mCherry sensor described earlier[24], Mtb episomally expressing replication probe SSB-GFP[22], a kind gift from Dr. David Russell, CDC1551 clinical strain of Mtb (NR-13649, BEI resource). All these strains were cultured in 7H9 medium (Becton Dickinson, Difco, 271310) containing 0.2% glycerol, 0.1% Tween 80 (MP Biomedical, 103170), and 10% OADC (Oleic acid, BSA fraction V, Dextrose, Catalase, and NaCl), till the optical density reached 0.8–1.0 at 600 nm. The culture was centrifuged at 3220 x *g* for 10 min, followed by resuspension of the pellet in a freezing medium (complete 7H9 + 20% glycerol [Fisher Scientific, 15457]). Cultures were maintained using antibiotics such as Hygromycin (Hyg, 50 μg/ml), and Kanamycin (Kan, 20 μg/ml). CFU plating was performed to estimate the number of viable cells. Cultures were aliquoted and stored at −80 °C. All the experiments were performed using these stocks. For heat killing

Fig. 7 | TFEB-TMEM55B-JIP4 axis drives retrograde lysosomal trafficking mediated by IFN-γ. a THP-1 macrophages were treated with control siRNA or TMEM55B siRNA infected with GFP-MtbH37Rv. Cells were stimulated with or without IFN-γ. Violin plots depicting the distribution of GFP-MtbH37Rv in macrophage cells as perinuclear index (**b**, $n > 44$) and fractional distance (**c**, $n > 90$) (One-tailed, Mann–Whitney U test, CI-95%). **d** THP-1 macrophages were treated with control siRNA or TMEM55B siRNA, infected with GFP-MtbH37Rv, and stimulated with or without IFN-γ. Cells were stained for lysosomes with anti-LAMP1 antibody, and colocalization with Mtb-laden cargoes was monitored. The inset shows an enlarged region of interest containing Mtb to examine Mtb's delivery to lysosomes. **e** Percent colocalization of GFP-MtbH37Rv with lysosomes (stained with anti-LAMP1 antibody) ($n = 60$) was quantified from experiments described in panel d (One-tailed, unpaired Student's *t* test, CI-95%). **f** MtbH37Rv survival in THP-1 macrophages treated with control siRNA or TMEM55B siRNA and stimulated with or without IFN-γ post-infection was calculated through CFU estimation (One-tailed, unpaired Student's *t* test, CI-95%). **g** THP-1 macrophages were treated with control siRNA or JIP4 siRNA, infected with GFP-MtbH37Rv, and stimulated with or without IFN-γ. Violin plots depicting the distribution of GFP-MtbH37Rv as a perinuclear index (**h**, $n > 55$) and fractional distance (**i**, $n > 90$) (One-tailed, Mann–Whitney U test, CI-95%). **j** THP-1 macrophages were treated with control siRNA or JIP4 siRNA, infected with GFP-MtbH37Rv and stimulated with or without IFN-γ. Cells were stained for lysosomes with anti-LAMP1 antibody, and colocalization with Mtb-laden cargoes was monitored. **k** Percent colocalization of GFP-MtbH37Rv with lysosomes (stained with anti-LAMP1 antibody) ($n = 36–50$) was quantified from experiments described in **j** (One-tailed, unpaired Student's *t* test, CI-95%). **l** MtbH37Rv survival in THP-1 macrophages treated with control or JIP4 siRNA and stimulated with or without IFN-γ post-infection was calculated through CFU estimation (One-tailed, unpaired Student's *t* test, CI-95%). Data in **b**, **c**, **h**, **i** represent Mtb distribution in four quarters (with median (central line), first quartile (upper line), and third quartile (lower line) from three independent biological experiments. Data in **e**, **f**, **k**, **l** represent mean ± SEM from three independent biological experiments. Scale Bar: 10 μm.

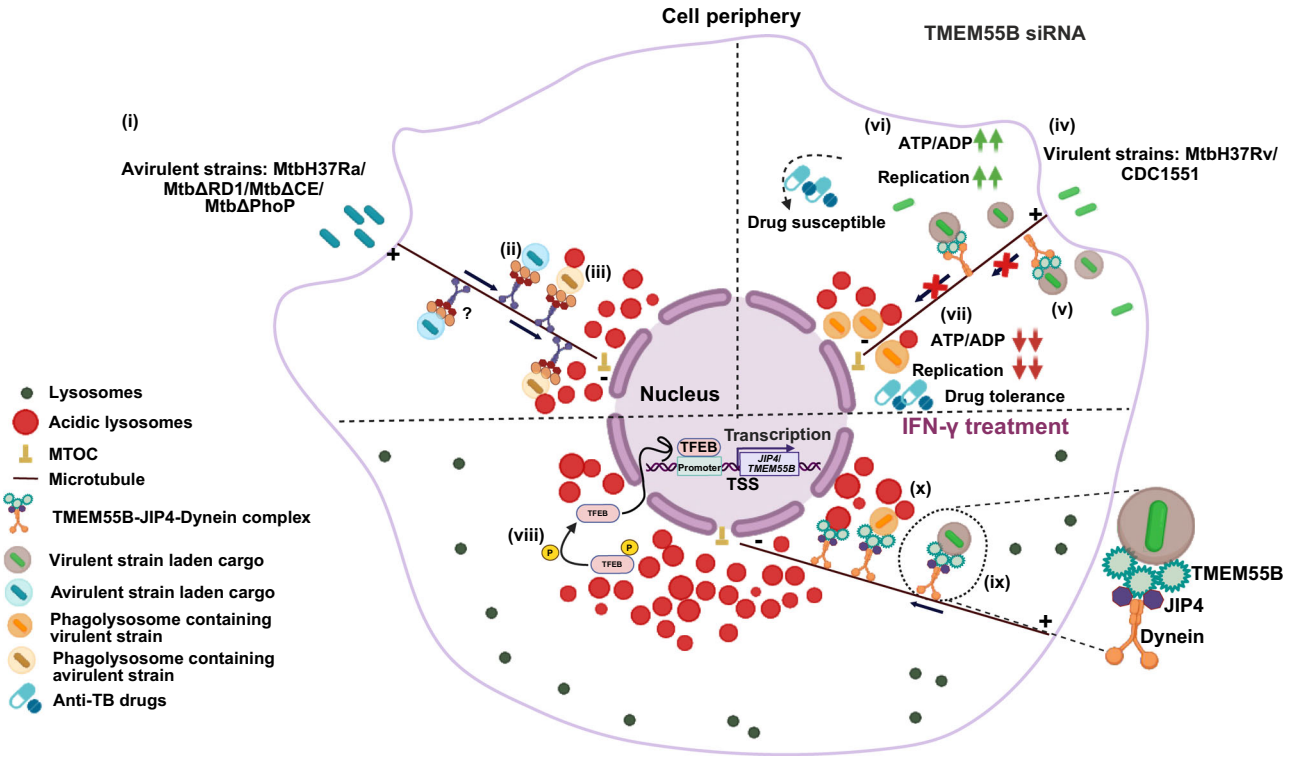

Fig. 8 | Model depicting effect of spatial localization of *M. tuberculosis* on its physiology, delivery to lysosomes, and survival inside macrophages. (i) Phagocytosis of avirulent strains of mycobacteria, i.e., MtbH37Ra, MtbΔRD1, MtbΔCE, and MtbΔPhoP. (ii and iii) Retrograde transport of avirulent strains of mycobacteria towards the perinuclear region of the cell and their fusion with lysosomes. The avirulent strain of mycobacteria is unable to inhibit the retrograde transport towards the perinuclear region where the fusion rate of phagosomes and lysosomes is higher, and hence the chance of its killing increases. (iv) Phagocytosis of virulent strains of mycobacteria, i.e., MtbH37Rv and CDC1551. (v) Virulent strains inhibit the retrograde transport of cargo containing it. (vi) Mtb cells localized at the cell periphery have higher metabolic rates (ATP/ADP levels), higher replication rates, and are drug-susceptible. (vii) Mtb cells localizing in the perinuclear region have a lower metabolic rate (ATP/ADP levels), replication rate, and are drug-tolerant, thus representing the persister population. (viii) IFN-γ induces dephosphorylation of TFEB, inducing its translocation into the nucleus, where it binds to the CLEAR motif of the *JIP4* and *TMEM55B* promoter region and starts their transcription. (ix and x) JIP4 and TMEM55B mediate the retrograde transport of Mtb-laden cargo towards the perinuclear region where fusion with lysosomes occurs. This figure illustrates the role of virulence factors regulating the subcellular localization of mycobacteria, which dictates its bioenergetic state and replication status; this in turn is responsible for differential response towards the anti-TB drug in the same macrophage. This figure also depicts the TMEM55B-JIP4-dynein axis for regulating IFN-γ-mediated perinuclear localization of Mtb-laden cargo. The model shown in the figure was created using BioRender.com.

of MtbH37Rv, stocks were centrifuged at 3200 x *g* for 10 min, and the pellet obtained was resuspended in RPMI 1640. The resuspended pellet was kept at 80 °C for 30 min and used for the experiment. All Mtb experiments were conducted in a BSL-3 facility (CSIR-IMTech, Chandigarh), strictly following standard operating procedures approved by institutional biosafety committee of CSIR-Institute of Microbial Technology.

Generation of mCherry-MtbH37Rv

MtbH37Rv strain was transformed with a pMV762-mCherry plasmid (episomal plasmid use *hsp60* promoter in mycobacteria), and bacteria were selected on 7H11 agar plate containing hygromycin B (50 μg/ml) and 10% OADC. A single transformed bacterial colony was inoculated in 7H9 medium supplemented with 0.2% glycerol, 0.1% Tween 80, and 10% OADC with 50 μg/ml of hygromycin B.

In vivo, infection and lung perfusion. 8-week-old C3HeB/FeJ mice (breeding pairs) were procured from Jackson Laboratory (USA) and bred at Animal Colony Maintenance facility, under specific pathogen-free containment. Three mice required were shifted to Animal-BSL3 for infection and further experiments. Animals were kept in an Individual Ventilated Cages (IVC) system with a 60 air change per hour cycle. Cages were kept in a room having controlled temperature (22 ± 2 °C) and light: dark cycle (14:10 h) and humidity of 45–60%. Ad libitum water and food pellets (SAFE® D131) were provided. Mice infections were performed using the Glas-Col inhalation exposure system with an initial dose leading to around 200 CFU/lung deposition in each mouse. Mice were sacrificed 2 weeks post-infection. During the sacrifice process, the mice's lungs were perfused with PBS through the right ventricle of the heart to remove blood from the lungs. After perfusion, the lungs were dissected out and fixed with 4% formaldehyde overnight for further experiments.

Lung tissue sectioning, immunostaining, imaging, and analysis. Formaldehyde fixed lungs were sectioned (20 μm) using Cryostat-MEV (SLEE Medical). For immunofluorescence staining, lung sections were permeabilized using SAP buffer (0.2% saponin (Sigma-Aldrich S4521)), and 0.2% gelatin (HiMedia Laboratories TC041) in PBS for 15 min at room temperature. Primary antibody (LAMP1 (DSHB, 1D4B) was prepared in SG-PBS (0.02% saponin and 0.2% gelatin in PBS)) and incubated for 1 h at room temperature. Saponin in these buffers was used as a detergent and gelatin as a blocking agent. Tissue sections were washed with SG-PBS and incubated with Alexa-tagged secondary antibodies that were prepared in SG-PBS for 1 h at room temperature. After washing with SG-PBS, sections were counterstained with DAPI and phalloidin, and slides were mounted with Mowiol (Sigma-Aldrich) and imaged using a confocal microscope, Olympus-FV3000.

BMDMs isolation and culture

BMDMs were isolated from the femur, tibia, and fibula of the C57BL6 mice (male). Mice were first sacrificed by cervical dislocation, and then the desired bones were isolated and disinfected with 70% ethanol. Disinfected bones were punctured using a syringe by passing 1× PBS (NaCl, KCl, Na_2HPO_4, and KH_2PO_4, pH 7.4). Isolated bone marrow was centrifuged at 69 x *g* for 5 min, and the pellet was treated with ACK lysis buffer to remove red blood cells. Followed by 1× PBS washing and culturing BMDMs in RPMI 1640 media supplemented with 10% fetal bovine serum (FBS), 1% Penicillin-Streptomycin, β-mercaptoethanol, essential amino acids, and 20 ng/ml of purified macrophage colony-stimulating factor.

Cell culture

Human THP1-monocytes were procured from ATCC (ATCC TIB-202) and were cultured in RPMI 1640 media supplemented with 10% FBS at 37 °C under 5% CO_2. Monocytes were differentiated for 24 h with 30 ng/ml of phorbol 12-myristate 13-acetate (PMA) and after 48 h of recovery in PMA-free RPMI medium, further experiments were performed.

Transfection and treatments

The desired siRNA was transfected into THP1 macrophages using Lipofectamine™ RNAiMax transfection reagent as per the manufacturer's protocol. Briefly, the siRNA and Lipofectamine™ RNAiMax were prepared in Opti-MEM and added to the cells drop-wise. Complete media was added before the addition of the transfection mixture. The list of siRNAs used is enlisted in Supplementary Table 3.

Recombinant human IFN-γ and mouse IFN-γ were procured from R&D systems. THP1 macrophages were treated with human IFN-γ (500 units/ml) for 3 h. Followed by washing the cells with 1× PBS. Similarly, BMDM macrophages were treated with mouse IFN-γ (200 units/ml) for 3 h. THP1-macrophages were treated with Ciliobrevin D (20 μM for 2 h) before infection.

Antibiotics treatment

THP1 macrophages (0.10×10^6) were plated in 24-well plates and infected with GFP-MtbH37Rv, (1:10 MOI) for 3 h, treated with 100 μg/ml gentamicin for 30 min (to remove extracellular bacilli) and then treated with anti-tuberculosis drugs such as Rifampicin (Himedia Laboratories, CMS1889), Isoniazid (MedChemExpress, HY-B0329) at (5× Minimal Inhibitory Concentration) containing 20 μg/ml gentamicin media for 48 h. Forty eight hours post-infection, cells were washed with 1X PBS and fixed with 4% paraformaldehyde (PFA). Further nucleus was counterstained with DAPI for 15 min at room temperature. After washing with PBS, the coverslips were mounted using Slowfade™ Diamond Antifade Mountant. Confocal images were acquired using a Nikon A1R Confocal laser Scanning Microscope using a 60×/1.0 NA oil immersion objective. NIS element software was used to acquire the images. Images were analyzed through Fiji software.

Lysate preparation, immunoblotting and immunoprecipitation

Following treatments, cells were washed thrice with 1× PBS. Cells lysis was done using ice-cold RIPA lysis buffer (10 mM Tris-Cl pH 8.0, 1 mM EDTA, 0.5 mM EGTA,1% Triton X-100, 140 mM NaCl, 0.1% sodium deoxycholate, and 0.1% SDS, containing protease inhibitor cocktail (Roche, 589270001) for 5 min on ice. Lysed cells were centrifuged at 30,000 x *g* for 10 min at 4 °C, and the supernatant was collected. A bicinchoninic acid assay (BCA) kit was used for protein estimation, containing BCA solution (B9643) and CuSO4 (C2284) from Sigma Aldrich. Samples were prepared by boiling the desired concentration of protein with 4× Laemmli buffer (Tris-Cl 1.0 M, pH = 6.8); 40% glycerol; SDS; *β-mercaptoethanol;* bromophenol blue). Boiled samples were run on SDS-PAGE and transferred to PVDF membrane (MDI Membrane Technologies, SVFX8301XXXX101). Membrane was blocked using 5% BSA for 2 h at room temperature. The membrane was then washed thrice with PBST (0.1% Tween20) and incubated with primary antibodies against TFEB, JIP4, TMEM55B, and β-actin antibodies overnight at 4 °C. Post washing, blots were incubated with respective secondary antibodies: Goat Anti-Rabbit IgG (H + L)-HRP Conjugate and Rabbit Anti-Mouse IgG (whole molecule)-HRP antibody. Blots were developed using enhanced chemiluminescence (ECL) Luminata forte (Merck, WBLUF0500) and exposed to X-ray retina film (XBE X-ray film, 6574958) to visualize bands.

To perform co-immunoprecipitation, cells from 10 cm dishes were subjected to lysis buffer (150 mM NaCl [Invitrogen, AM9759], 50 mM Tris [Invitrogen, AM9850G], pH 7.0, 1 mM EDTA [Invitrogen, AM9260G], and 1% Triton X-100 [Sigma Aldrich,78787]) containing protease inhibitor cocktail and incubated overnight with JIP4 antibody conjugated to amino linked beads at 4 °C with gentle rotation. Co-immunoprecipitation was performed as per the manufacturer's protocol using an amino link co-immunoprecipitation kit. Immunocomplexes were separated by SDS-PAGE and detected through immunoblotting using JIP4 and TMEM55B as primary antibodies. Secondary Goat Anti-Rabbit IgG (H + L)-HRP Conjugate and Rabbit Anti-Mouse IgG (whole molecule)-HRP antibody were used to detect the bands. Blots were developed using ECL Luminata Forte and exposed to X-ray retina film for visualization of bands.

ChIP assay

Monocytes were differentiated for 24 h with 30 ng/ml of PMA and after 48 h of recovery in PMA-free RPMI medium, cells were treated with IFN-γ for 3 h. Further, cross-linking of the protein-DNA complex was performed using 1% formaldehyde for 10 min. Crosslinking was quenched by adding 125 mM glycine for 5 min at room temperature. Subsequently, prior to cell lysis, the cells were washed thrice with cold 1× PBS. Cells were resuspended in ChIP lysis buffer (50 mM Tris pH 8.1,

85 mM KCl, 0.5% NP40, and 1× PIC) and sonicated in bath sonicator for 20 min (30 s Off-On, on low amplitude) till 200–500 base pair DNA fragment were achieved. Lysate was ultracentrifuged at 12,000 x *g* at 4 °C, and supernatant was collected. Supernatant was diluted in 2× IP dilution buffer (0.02% SDS, 2.2% Triton X 100, 2.4 mM EDTA, 33.4 mM Tris pH 8.1, 167 mM NaCl,167 mM LiCl) and the pre-clearing was performed using equal amount of Protein A&G beads for 1 h, respectively. Out of the total volume, 10% of it was kept as input and the rest was kept for binding with 10 μg Anti-TFEB antibody overnight. Next day, mixture of A&G magnetic beads (BIO-RAD G beads Cat. #161-4023 A beads #161-4013) was added to each tube and kept on nutator at 4 °C 3 h. Beads were washed twice for 5 min at room temperature with 1× IP Dialysis Buffer (2 mM EDTA and 50 mM Tris pH 8) and three times with IP wash buffer (100 mM Tris pH 8, 250 mM LiCl, 1% NP-40, and 1% Na-deoxycholate) for 5 min at room temperature. Quick wash with 1× TE Buffer (10 mM Tris-HCl pH 8 and 1 mM EDTA) and bound DNA fragments were eluted twice using elution buffer (50 mM $NaHCO_3$ and 1% SDS) at 65 °C. Input and eluted DNA were heated at 65 °C overnight for reverse crosslinking, which was followed by RNase treatment and finally the proteinase K treatment. DNA samples were purified using Phenol Chloroform extraction method. Samples were run on 1.2% agarose gel in 1× TAE buffer.

Colony forming unit assay

THP1-monocytes (1×10^6) were plated in a 6-well plate and incubated for 24 h in a CO_2 incubator at 37 °C. Cells were transfected with the desired siRNA, and knockdown was performed for 48 h. siRNA-treated cells were infected with MtbH37Rv and MtbH37Ra (1:10 MOI) for 3 h and treated with 100 μg/ml gentamicin (Gibco, 15710064) for 30 min (to remove extracellular bacilli) and then stimulated with IFN-γ (500 units/ml) containing 20 μg/ml gentamicin media. After 48 h cells were lysed using 0.06% SDS, serially diluted in PBS, and plated on Middlebrook 7H11(Becton Dickinson Difco™, 212203) plates supplemented with 10% OADC. The plates were incubated at 37 °C, and bacterial colonies were counted after 2–3 weeks. CFU was enumerated and plotted using GraphPad Prism v8.0.

Immunostaining and confocal microscopy

After fixation with 4% PFA, cells were incubated in the primary antibody (Anti-LAMP1 antibody), at room temperature for 2 h (described in legends) which was prepared in staining solution (0.25% saponin w/v and 1% bovine serum albumin w/v in PBS), followed by three washes and then incubated in Alexa-Fluor conjugated 488/568/647 goat anti rabbit-IgG prepared in staining solution for 45 min at room temperature. The nucleus was counterstained with Hoechst for 15 min at room temperature. After washing with PBS, coverslips were mounted using Slowfade™ Diamond Antifade mountant. Confocal images were acquired using a Nikon A1R Confocal laser Scanning Microscope using a 60×/1.0 NA oil immersion objective. NIS element software was used to acquire the images. Images were analyzed through Fiji software.

Transmission electron microscopy

THP1 macrophages were infected with MtbH37Rv, MtbH37Ra, and MtbΔRD1 (1:10 MOI) for 3 h, treated with 100 μg/ml gentamycin for 30 min (to remove extracellular bacilli) and then incubated in 20 μg/ml gentamicin containing media for 3 h. Similarly, for another experiment, cells were infected with MtbH37Rv, as mentioned above and then stimulated with IFN-γ (500 units/ml) containing 20 μg/ml gentamycin media. DPBS was used for washing after treatment. Cells were then fixed in PBS containing 4% PFA and 2% glutaraldehyde (Sigma Aldrich, 111308) for 1 h at 4 °C. Post fixation, cells were collected using a cell scraper, pelleted down at 800 x *g* for 10 min and proceeded for TEM processing at CSIR-IMTech, Chandigarh. Cells were washed twice in 0.1 M cacodylate buffer and subjected to dehydration with an acetone gradient (30%, 50%, 70%, 80%, and 90%) for 30 min. Briefly, the specimen was kept in absolute acetone for 1 h at 4 °C. The specimen was embedded in epoxy resin for 36 h at 55 °C. Ultrathin sections (80 nm) were prepared using an ultramicrotome (LEICA EM UC7) and collected on copper grids. Sections were stained with 2% uranyl acetate (alcoholic) and examined in TEM (JEOL JEM-2100).

Dextran trafficking assay

Cells were incubated with Alexa-Fluor 647 conjugated Dextran (0.25 mg/ml) to label the lysosomes (pulse) overnight at 37 °C under 5% CO_2 condition. Treated cells were washed thrice with DPBS and kept in complete RPMI 1640 media for 3 h for the chase. Briefly, to label the acidic lysosomes, IFN-γ-treated and untreated cells were incubated with LysoTracker Red (100 nM) for 1 h at 37 °C under 5% CO_2. After the incubation, cells were washed with PBS, followed by fixation and mounting, as explained earlier. The colocalization index (Pearson's coefficient and Mander's coefficient) of dextran with LysoTracker-labeled lysosomes was obtained through the JACoP plugin in Fiji software.

Time-lapse imaging

For live cell imaging, the cells were seeded on the 8-chambered glass slide. For imaging, cells were incubated with Alexa-Fluor 647 conjugated Dextran (0.25 mg/ml) to label the lysosomes (pulse) overnight at 37 °C under 5% CO_2. After the treatment cells were washed thrice with DPBS and kept in complete RPMI 1640 media for 3 h for the chase. Imaging of cells was performed in a Nikon A1R Confocal laser Scanning Microscope using 60×/1.0 NA oil immersion objective. Live cell imaging of untreated cells was carried out for 5 min, after which the same chambered glass slide was incubated with the IFN-γ-containing media, and then the imaging was performed for the IFN-γ panel. The images were acquired at a rate of 10 s for each frame for 1 h.

RNA isolation and qRT-PCR

RNA was isolated after the IFN-γ treatment by using the TRIzol reagent method. The cDNA synthesis and qRT-PCR were performed using SuperScript III Platinum™ SYBR™ Green One-Step qRT-PCR Kit using 50 ng of total RNA as a template. TMEM55B, and JIP4 gene expression levels were analyzed by qRT-PCR using gene-specific primers enlisted in Supplementary Table 4 using β actin as a housekeeping gene. Briefly, cDNA synthesis was performed at 50 °C for 3 min. The qRT-PCR cycle comprises initial denaturation at 95 °C for 5 min, 45 cycles of denaturation at 95 °C for 15 s, annealing at 60 °C for 45 s, and extension at 40 °C for 45 s (using Bio-Rad CFX96 Touch Real-Time PCR Detection System). The melt curve was performed from 60 to 90 °C with a 0.3 °C increase per step. The relative quantification in gene expression levels was determined using the ΔΔCt method[73].

Lysosomal enrichment

The enrichment of lysosomes was performed by using Lysosome Enrichment Kit (Thermo Scientific, 89839) for tissues and cultured cells. IFN-γ-treated (500 Units) and untreated THP-1 macrophages were collected and washed thrice with 1× PBS. Cells were detached by using PBS-EDTA (10 mM), scraped, and harvested at 850 × *g* for 5 min. Cells were lysed by resuspending the pellet in buffer A (protease inhibitor cocktail, PIC dissolved), and syringe passed around 15 times (until 8 out of every 10 cells were found to be ruptured). The lysate was subjected to lysis by adding buffer B + PIC. The lysate was then centrifuged at 500 × *g* for 10 min at 4 °C. The obtained supernatant was loaded onto a pre-laid Opti density gradient (30%/27%/24%) in an ultracentrifuge tube. The gradient was centrifuged at 53,300 x *g* for 4 h at 4 °C. The topmost layer of organelles was then carefully pipetted out and proceeded to the western blot for confirmation (anti-JIP4, anti-LAMP1 antibody, anti-Cytoplasmic Dynein Intermediate Chain antibody and anti-TMEM55B). Secondary Rabbit Anti-Mouse IgG

(whole molecule)-HRP antibody and Goat Anti-Rabbit IgG (H + L)-HRP Conjugate were used to detect the bands.

Analysis of lysosome distribution

The methodology for the calculation of the perinuclear index was adapted from ref. 27. Fiji software was used to quantify the distribution of lysosomes based on LAMP1 signal intensity. Lysosome distribution was analyzed in macrophages with an area above 500 μm^2. Cell boundary was drawn by making the region of interest (ROI) (first ROI) using a freehand selection tool, and nearby LAMP1 intensity was removed using the clear outside function of Fiji software. LAMP1 intensity for the whole cell was termed as I_{total}. Next nuclear ROI (second ROI) was also drawn using Hoechst intensity. The same ROI was expanded by 3 μm (third ROI) and 6 μm (fourth ROI). The LAMP1 intensity was measured for perinuclear ($I_{perinuclear}$) (subtracting the LAMP1 intensity of the second ROI from the third) and the area beyond 6 μm from the nucleus was denoted as $I_{peripheral}$ (by subtracting the intensity of the fourth ROI from the first). The perinuclear and peripheral intensities were normalized as $I < 3 = I_{perinuclear}/I_{total} - 100$ and $I > 6 = I_{peripheral}/I_{total} - 100$, respectively. The perinuclear index was calculated by subtracting the normalized intensity within 3 μm distance from the normalized intensity beyond 6 μm distance ($I < 3 - I > 6$). Same data was plotted using Graph Pad Prism v8.0.

Analysis of Mtb distribution in infected macrophages

The perinuclear index analysis was performed similar to the analysis of lysosome distribution. Here, the total intensity of GFP-Mtb/mCherry-Mtb was calculated within the specified ROI, and the perinuclear index was calculated by subtracting the normalized intensity within 3 μm distance to the normalized intensity beyond 6 μm distance ($I < 3 - I > 6$). The same was plotted using Graph Pad Prism v8.0.

For the fractional distance analysis, we drew a linear distance from the nucleus to the cellular periphery, followed by the extraction of the fluorescence plot profile from which fluorescence intensity and distance values along the line were taken out for calculation. The distance from nucleus to cellular periphery was ranged between 0 and 1. Fractional distance was calculated by dividing all the values from the total cell distance. Mtb cells with greater than 300 Gray values were utilized in this calculation. The same was plotted using Graph Pad Prism v8.0.

Calculation of ATP/ADP levels of MtbH37Rv spatially in macrophages

Infected macrophages with PHR-mCherry strain of MtbH37Rv were randomly chosen, ROI was drawn for the bacteria and its localization was measured by drawing concentric rings around the nucleus of 3 μm, 6 μm, 9 μm, and beyond 9 μm. Through this, we were able to mark the bacterial location in the macrophages. After this, we calculated the integrated density coming from the bacteria at 488 nm channels (PHR) and 561 nm channels (mCherry). These values were extracted from ImageJ. Ratiometric values were calculated by dividing 488/561 integrated density values, which denotes the ATP/ADP ratio of that bacteria. The number of bacteria was randomly chosen as described below through an online platform. This way, the level of ATP/ADP was calculated for the bacteria localized at different distances and plotted using GraphPad Prism v8.0.

Calculation of % MtbH37Rv showing SSB replication foci spatially in macrophages

Infected macrophages with SSB- MtbH37Rv were randomly chosen, ROI was drawn for the bacteria, and its localization was measured by drawing concentric rings around the nucleus of 3 μm, 6 μm, 9 μm and beyond 9 μm. Through this, we were able to mark the bacterial location in the macrophages. We calculated the bacteria showing SSB replication foci and marked them as 1, and the bacteria not showing SSB replication foci as 0. The number of bacteria showing foci was divided by the total number of bacteria in that concentric ring. The number of bacteria was randomly chosen as described below through an online platform, and the percentage of bacteria showing SSB replication foci was plotted using GraphPad Prism v8.0.

Analysis of percentage population of GFP-Mtb in macrophages

GFP-MtbH37Rv distribution was quantified using Fiji software, where macrophages with an area above 500 μm^2 were selected. Cell boundary was made by drawing the ROI (first ROI) using a freehand selection tool, and intensity from surrounding GFP-Mtb was removed using the clear outside function in Fiji software. Next nuclear ROI (second ROI) was drawn using Hoechst intensity. The same ROI was expanded by 3 μm (third ROI), 6 μm (fourth ROI), 9 μm (fifth ROI), and beyond 9 μm. The number of bacteria in each ROI was manually calculated and plotted in terms of percentage in GraphPad Prism v8.0.

Analysis of colocalization of lysosome with GFP-Mtb in infected macrophages

Colocalization of GFP-MtbH37Rv and lysosomes was analyzed through percent colocalization, Pearson's coefficient, and Mander's coefficient. Lysosomes in infected macrophages were stained with LAMP1 antibody, as mentioned above. For percent colocalization, the number of yellow (colocalized) bacteria and green bacteria was calculated.

$$\text{Percent colocalization} = \frac{\text{Number of yellow bacteria}}{\text{Total number of bacteria}} \text{X100}$$

JACoP plugin from Fiji was used for calculating Pearson's coefficient and Mander's coefficient.

Analysis of lysosome area

Cells were randomly chosen to calculate the lysosomal area. Cell boundary was made by drawing the ROI using the freehand selection tool, and nearby LAMP1 intensity was removed using the clear outside function of Fiji software. The threshold of LAMP1 positive punctate was adjusted accordingly to cover all the lysosomes in the selected ROI. Analyzed particles were used to measure the area of all the lysosomes in the cell. Graph Pad Prism v8.0 was used to plot the average of all the lysosome's area from a particular cell.

Analysis of linear distance of GFP-MtbH37Rv in macrophages

Infected macrophages were randomly chosen, and a linear distance from the center of the nucleus to the bacteria (first ROI) and cell periphery (second ROI) was drawn. The relative distance of bacteria was calculated by dividing the first ROI by the second ROI.

Analysis of live cell imaging

Time-lapse imaging was performed as described above. To measure the displacement and maximum speed attained by the lysosomes from time-lapse images, the TrackMate plugin[74] from Fiji was used with the below-mentioned parameters:

Vesicle diameter: 3 μm
Quality threshold: 7
Detector: DoG
Initial thresholding: Auto
Tracker: Simple LAP tracker
Linking max distance: 15 μm
Gap closing max distance: 15 μm
Gap closing max frame gap: 4
Filters: none

Data were exported in the file format of .csv which was converted into a Microsoft excel spreadsheet (2013).

Randomization of the number of Mycobacteria using an online tool

During the calculation of ATP/ADP levels or % of Mtb showing SSB replication foci at different distances with respect to the nucleus of macrophages i.e., 0–3 μm, 3–6 μm, 6–9 μm and beyond 9 μm from different biological replicates, we found a different number of bacteria at each distance. So, to nullify the biases, we opted for an online randomization (https://usegalaxy.org/) tool where the number of bacteria to be selected from all the biological replicates was fixed, and the command was set to choose that particular number of bacteria from each distance and the values were plotted using GraphPad Prism v8.0.

Violin plot preparation

Violin plots were generated using ggplot2 command lines for quartile violin plots in R software. Violin plots shown in the manuscript represents median line (central line), first quartile (lower line), and 3rd quartile (upper line) for the respective distribution.

Software used in the study

The statistical test and graphs were prepared using GraphPad Prism 8. Manuscript figures were prepared in Corel Draw 2020 and Biorender: scientific and image illustration software. Representative confocal images were adjusted for brightness and contrast using Image software (Fiji v 2.3.0).

Statistical analysis

The statistical significance was determined by applying an unpaired, non-parametric Mann–Whitney U test for data in PNI and fractional distance calculation ($n < 30$) and unpaired, parametric Student's t test for data in percentage population, percent colocalisation and CFU analysis ($n > 10$). $^{*}p < 0.05$, $^{**}p < 0.01$, $^{***}p < 0.001$ and $^{****}p < 0.0001$ were considered statistically significant.

Reporting summary

Further information on research design is available in the Nature Portfolio Reporting Summary linked to this article.

Data availability

All relevant information supporting the findings of this study is presented in the manuscript and supplementary materials. A source file comprising raw data and western blot images that have not been cropped is included in the manuscript. Source data are provided with this paper.

References

1. World Health Organization. *Global tuberculosis report 2022* (WHO, 2022).
2. Gutierrez, M. G. et al. Autophagy is a defense mechanism inhibiting BCG and Mycobacterium tuberculosis survival in infected macrophages. *Cell* **119**, 753–766 (2004).
3. Vergne, I., Chua, J., Singh, S. B. & Deretic, V. Cell biology of mycobacterium tuberculosis phagosome. *Annu. Rev. Cell Dev. Biol.* **20**, 367–394 (2004).
4. van der Wel, N. et al. *M. tuberculosis* and *M. leprae* translocate from the phagolysosome to the cytosol in myeloid cells. *Cell* **129**, 1287–1298 (2007).
5. Kinchen, J. M. & Ravichandran, K. S. Phagosome maturation: going through the acid test. *Nat. Rev. Mol. Cell Biol.* **9**, 781–795 (2008).
6. Christoforidis, S. et al. Phosphatidylinositol-3-OH kinases are Rab5 effectors. *Nat. Cell Biol.* **1**, 249–252 (1999).
7. Murray, J. T., Panaretou, C., Stenmark, H., Miaczynska, M. & Backer, J. M. Role of Rab5 in the recruitment of hVps34/p150 to the early endosome. *Traffic* **3**, 416–427 (2002).
8. Armstrong, J. A. & Hart, P. D. Response of cultured macrophages to *Mycobacterium tuberculosis*, with observations on fusion of lysosomes with phagosomes. *J. Exp. Med.* **134**, 713–740 (1971).
9. Ishibashi, Y. & Arai, T. Effect of gamma-interferon on phagosome-lysosome fusion in *Salmonella typhimurium*-infected murine macrophages. *FEMS Microbiol. Immunol.* **2**, 75–82 (1990).
10. Russell, D. G. *Mycobacterium tuberculosis*: here today, and here tomorrow. *Nat. Rev. Mol. Cell Biol.* **2**, 569–577 (2001).
11. Armstrong, J. A. & Hart, P. D. Phagosome-lysosome interactions in cultured macrophages infected with virulent tubercle bacilli. Reversal of the usual nonfusion pattern and observations on bacterial survival. *J. Exp. Med.* **142**, 1–16 (1975).
12. Alsaadi, A. I. & Smith, D. W. The fate of virulent and attenuated Mycobacteria in guinea pigs infected by the respiratory route. *Am. Rev. Respir. Dis.* **107**, 1041–1046 (1973).
13. McDonough, K. A., Kress, Y. & Bloom, B. R. Pathogenesis of tuberculosis: interaction of *Mycobacterium tuberculosis* with macrophages. *Infect. Immun.* **61**, 2763–2773 (1993).
14. Zhang, M., Gong, J., Lin, Y. & Barnes, P. F. Growth of virulent and avirulent *Mycobacterium tuberculosis* strains in human macrophages. *Infect. Immun.* **66**, 794–799 (1998).
15. Lenaerts, A., Barry, C. E. 3rd & Dartois, V. Heterogeneity in tuberculosis pathology, microenvironments and therapeutic responses. *Immunol. Rev.* **264**, 288–307 (2015).
16. Cadena, A. M., Fortune, S. M. & Flynn, J. L. Heterogeneity in tuberculosis. *Nat. Rev. Immunol.* **17**, 691–702 (2017).
17. Chung, E. S., Johnson, W. C. & Aldridge, B. B. Types and functions of heterogeneity in mycobacteria. *Nat. Rev. Microbiol.* **20**, 529–541 (2022).
18. Savulescu, A. F. et al. Quantifying spatial dynamics of *Mycobacterium tuberculosis* infection of human macrophages using microfabricated patterns. *Cell Rep. Methods* **3**, 100640 (2023).
19. Abramovitch, R. B., Rohde, K. H., Hsu, F. F. & Russell, D. G. aprABC: a *Mycobacterium tuberculosis* complex-specific locus that modulates pH-driven adaptation to the macrophage phagosome. *Mol. Microbiol.* **80**, 678–694 (2011).
20. Tan, S., Sukumar, N., Abramovitch, R. B., Parish, T. & Russell, D. G. *Mycobacterium tuberculosis* responds to chloride and pH as synergistic cues to the immune status of its host cell. *PLoS Pathog.* **9**, e1003282 (2013).
21. Bhaskar, A. et al. Reengineering redox sensitive GFP to measure mycothiol redox potential of *Mycobacterium tuberculosis* during infection. *PLoS Pathog.* **10**, e1003902 (2014).
22. Sukumar, N., Tan, S., Aldridge, B. B. & Russell, D. G. Exploitation of *Mycobacterium tuberculosis* reporter strains to probe the impact of vaccination at sites of infection. *PLoS Pathog.* **10**, e1004394 (2014).
23. Bhat, S. A., Iqbal, I. K. & Kumar, A. Imaging the NADH:NAD(+) homeostasis for understanding the metabolic response of mycobacterium to physiologically relevant stresses. *Front. Cell Infect. Microbiol.* **6**, 145 (2016).
24. Akela, A. K. & Kumar, A. Bioenergetic heterogeneity in *Mycobacterium tuberculosis* residing in different subcellular niches. *mBio* **12**, e0108821 (2021).
25. Erie, C., Sacino, M., Houle, L., Lu, M. L. & Wei, J. Altered lysosomal positioning affects lysosomal functions in a cellular model of Huntington's disease. *Eur. J. Neurosci.* **42**, 1941–1951 (2015).
26. Johnson, D. E., Ostrowski, P., Jaumouille, V. & Grinstein, S. The position of lysosomes within the cell determines their luminal pH. *J. Cell Biol.* **212**, 677–692 (2016).
27. Li, X. et al. A molecular mechanism to regulate lysosome motility for lysosome positioning and tubulation. *Nat. Cell Biol.* **18**, 404–417 (2016).
28. Kumar, G. et al. RUFY3 links Arl8b and JIP4-Dynein complex to regulate lysosome size and positioning. *Nat. Commun.* **13**, 1540 (2022).

29. Tantama, M., Martinez-Francois, J. R., Mongeon, R. & Yellen, G. Imaging energy status in live cells with a fluorescent biosensor of the intracellular ATP-to-ADP ratio. *Nat. Commun.* **4**, 2550 (2013).
30. Reyes-Lamothe, R., Possoz, C., Danilova, O. & Sherratt, D. J. Independent positioning and action of *Escherichia coli* replisomes in live cells. *Cell* **133**, 90–102 (2008).
31. Ehrt, S., Schnappinger, D. & Rhee, K. Y. Metabolic principles of persistence and pathogenicity in *Mycobacterium tuberculosis*. *Nat. Rev. Microbiol.* **16**, 496–507 (2018).
32. Beatty, W. L. et al. Trafficking and release of mycobacterial lipids from infected macrophages. *Traffic* **1**, 235–247 (2000).
33. Fratti, R. A., Chua, J., Vergne, I. & Deretic, V. *Mycobacterium tuberculosis* glycosylated phosphatidylinositol causes phagosome maturation arrest. *Proc. Natl. Acad. Sci. USA* **100**, 5437–5442 (2003).
34. Garces, A. et al. EspA acts as a critical mediator of ESX1-dependent virulence in *Mycobacterium tuberculosis* by affecting bacterial cell wall integrity. *PLoS Pathog.* **6**, e1000957 (2010).
35. Walters, S. B. et al. The *Mycobacterium tuberculosis* PhoPR two-component system regulates genes essential for virulence and complex lipid biosynthesis. *Mol. Microbiol.* **60**, 312–330 (2006).
36. Guinn, K. M. et al. Individual RD1-region genes are required for export of ESAT-6/CFP-10 and for virulence of *Mycobacterium tuberculosis*. *Mol. Microbiol.* **51**, 359–370 (2004).
37. Frigui, W. et al. Control of *M. tuberculosis* ESAT-6 secretion and specific T cell recognition by PhoP. *PLoS Pathog.* **4**, e33 (2008).
38. Malakar, B. et al. Phosphorylation of CFP10 modulates *Mycobacterium tuberculosis* virulence. *mBio* **14**, e0123223 (2023).
39. Firestone, A. J. et al. Small-molecule inhibitors of the AAA+ ATPase motor cytoplasmic dynein. *Nature* **484**, 125–129 (2012).
40. Garg, S. et al. Lysosomal trafficking, antigen presentation, and microbial killing are controlled by the Arf-like GTPase Arl8b. *Immunity* **35**, 182–193 (2011).
41. Rosa-Ferreira, C. & Munro, S. Arl8 and SKIP act together to link lysosomes to kinesin-1. *Dev. cell* **21**, 1171–1178 (2011).
42. Hofmann, I. & Munro, S. An N-terminally acetylated Arf-like GTPase is localised to lysosomes and affects their motility. *J. Cell Sci.* **119**, 1494–1503 (2006).
43. Boehm, U., Klamp, T., Groot, M. & Howard, J. C. Cellular responses to interferon-gamma. *Annu. Rev. Immunol.* **15**, 749–795 (1997).
44. Schroder, K., Hertzog, P. J., Ravasi, T. & Hume, D. A. Interferon-gamma: an overview of signals, mechanisms and functions. *J. Leukoc. Biol.* **75**, 163–189 (2004).
45. Schaible, U. E., Sturgill-Koszycki, S., Schlesinger, P. H. & Russell, D. G. Cytokine activation leads to acidification and increases maturation of Mycobacterium avium-containing phagosomes in murine macrophages. *J. Immunol.* **160**, 1290–1296 (1998).
46. Lah, T. T., Hawley, M., Rock, K. L. & Goldberg, A. L. Gamma-interferon causes a selective induction of the lysosomal proteases, cathepsins B and L, in macrophages. *FEBS Lett.* **363**, 85–89 (1995).
47. Hipolito, V. E. B. et al. Enhanced translation expands the endo-lysosome size and promotes antigen presentation during phagocyte activation. *PLoS Biol.* **17**, e3000535 (2019).
48. Via, L. E. et al. Effects of cytokines on mycobacterial phagosome maturation. *J. Cell Sci.* **111**, 897–905 (1998).
49. Singh, N. et al. Antimycobacterial effect of IFNG (interferon gamma)-induced autophagy depends on HMOX1 (heme oxygenase 1)-mediated increase in intracellular calcium levels and modulation of PPP3/calcineurin-TFEB (transcription factor EB) axis. *Autophagy* **14**, 972–991 (2018).
50. Willett, R. et al. TFEB regulates lysosomal positioning by modulating TMEM55B expression and JIP4 recruitment to lysosomes. *Nat. Commun.* **8**, 1580 (2017).
51. Sardiello, M. et al. A gene network regulating lysosomal biogenesis and function. *Science* **325**, 473–477 (2009).
52. Sun, J. et al. Mycobacterium bovis BCG disrupts the interaction of Rab7 with RILP contributing to inhibition of phagosome maturation. *J. Leukoc. Biol.* **82**, 1437–1445 (2007).
53. Barry, C. E. et al. The spectrum of latent tuberculosis: rethinking the biology and intervention strategies. *Nat. Rev. Microbiol.* **7**, 845–855 (2009).
54. Lavin, R. C. & Tan, S. Spatial relationships of intra-lesion heterogeneity in *Mycobacterium tuberculosis* microenvironment, replication status, and drug efficacy. *PLoS Pathog.* **18**, e1010459 (2022).
55. Walter, N. D. et al. Lung microenvironments harbor *Mycobacterium tuberculosis* phenotypes with distinct treatment responses. *Antimicrob. Agents Chemother.* **67**, e0028423 (2023).
56. Manina, G., Dhar, N. & McKinney, J. D. Stress and host immunity amplify *Mycobacterium tuberculosis* phenotypic heterogeneity and induce nongrowing metabolically active forms. *Cell Host Microbe* **17**, 32–46 (2015).
57. Bach, H., Papavinasasundaram, K. G., Wong, D., Hmama, Z. & Av-Gay, Y. *Mycobacterium tuberculosis* virulence is mediated by PtpA dephosphorylation of human vacuolar protein sorting 33B. *Cell Host Microbe* **3**, 316–322 (2008).
58. Walburger, A. et al. Protein kinase G from pathogenic mycobacteria promotes survival within macrophages. *Science* **304**, 1800–1804 (2004).
59. Pradhan, G., Shrivastva, R. & Mukhopadhyay, S. Mycobacterial PknG targets the Rab7l1 signaling pathway to inhibit phagosome-lysosome fusion. *J. Immunol.* **201**, 1421–1433 (2018).
60. Renshaw, P. S. et al. Conclusive evidence that the major T-cell antigens of the *Mycobacterium tuberculosis* complex ESAT-6 and CFP-10 form a tight, 1:1 complex and characterization of the structural properties of ESAT-6, CFP-10, and the ESAT-6*CFP-10 complex. Implications for pathogenesis and virulence. *J. Biol. Chem.* **277**, 21598–21603 (2002).
61. Bates, T. A. et al. ESAT-6 undergoes self-association at phagosomal pH and an ESAT-6-specific nanobody restricts *M. tuberculosis* growth in macrophages. *Elife* **12**, RP91930 (2024).
62. Laopanupong, T. et al. Lysosome repositioning as an autophagy escape mechanism by *Mycobacterium tuberculosis* Beijing strain. *Sci. Rep.* **11**, 4342 (2021).
63. Bakowski, M. A., Braun, V. & Brumell, J. H. Salmonella-containing vacuoles: directing traffic and nesting to grow. *Traffic* **9**, 2022–2031 (2008).
64. Harrison, R. E. et al. Salmonella impairs RILP recruitment to Rab7 during maturation of invasion vacuoles. *Mol. Biol. cell* **15**, 3146–3154 (2004).
65. Kaniuk, N. A. et al. Salmonella exploits Arl8B-directed kinesin activity to promote endosome tubulation and cell-to-cell transfer. *Cell Microbiol.* **13**, 1812–1823 (2011).
66. Steele-Mortimer, O., Meresse, S., Gorvel, J. P., Toh, B. H. & Finlay, B. B. Biogenesis of *Salmonella typhimurium*-containing vacuoles in epithelial cells involves interactions with the early endocytic pathway. *Cell Microbiol.* **1**, 33–49 (1999).
67. Ramsden, A. E., Mota, L. J., Munter, S., Shorte, S. L. & Holden, D. W. The SPI-2 type III secretion system restricts motility of Salmonella-containing vacuoles. *Cell Microbiol.* **9**, 2517–2529 (2007).
68. Braun, V. et al. Sorting nexin 3 (SNX3) is a component of a tubular endosomal network induced by Salmonella and involved in maturation of the Salmonella-containing vacuole. *Cell Microbiol.* **12**, 1352–1367 (2010).
69. Bujny, M. V. et al. Sorting nexin-1 defines an early phase of Salmonella-containing vacuole-remodeling during Salmonella infection. *J. Cell Sci.* **121**, 2027–2036 (2008).
70. Henry, T., Gorvel, J. P. & Meresse, S. Molecular motors hijacking by intracellular pathogens. *Cell Microbiol.* **8**, 23–32 (2006).
71. Harrison, R. E., Bucci, C., Vieira, O. V., Schroer, T. A. & Grinstein, S. Phagosomes fuse with late endosomes and/or lysosomes by

extension of membrane protrusions along microtubules: role of Rab7 and RILP. *Mol. Cell. Biol.* **23**, 6494–6506 (2003).
72. Roberts, E. A., Chua, J., Kyei, G. B. & Deretic, V. Higher order Rab programming in phagolysosome biogenesis. *J. Cell Biol.* **174**, 923–929 (2006).
73. Livak, K. J. & Schmittgen, T. D. Analysis of relative gene expression data using real-time quantitative PCR and the 2(-Delta Delta C(T)) method. *Methods* **25**, 402–408 (2001).
74. Ershov, D. et al. TrackMate 7: integrating state-of-the-art segmentation algorithms into tracking pipelines. *Nat. Methods* **19**, 829–832 (2022).

Acknowledgements

Authors are thankful to Mr. Aadit Kumar on pointing out the differences in mycobacterial positioning in different images. The authors are also thankful to Dr. David R. Sherman (University of Washington School of Medicine, Seattle) for providing MtbΔRD1 strain, Dr. Dibyendu Sarkar (CSIR-Institute of Microbial Technology, India) for providing *phoPR* disruption mutant (MtbΔPhoP) and MtbΔPhoP Complementary strain of *M. tuberculosis* H37Rv; Dr. Amit Singh (Indian Institute of Science, India) for providing MtbH37Rv strain integrated with roGFP2; Dr. David Russell (Cornell University College of Veterinary Medicine, New York) for providing SSB-GFP, smyc'::: mCherry (SSB'::GFP fusion cloned in replicating plasmid pCherry3) plasmid construct Δ; Vinay Nandicoori (National Institute of Immunology, India) for MtbΔCE and MtbΔCE complementary strain. We are grateful to Mr. Rajkumar for taking care of ordering reagents and chemicals. A.K. is supported through Grant No. IA/S/20/2/505220 by DBT Wellcome Trust India Alliance . S.S., N.B., and A.P.D. were supported through a senior research fellowship by the Department of Biotechnology (DBT). M.G. was supported through DBT Wellcome Trust India Alliance as project assistant. D.A., Ankita S and Anunay S were supported through a junior and/or SRF by the University Grant Commission (UGC). S.M. is supported by senior research fellowship by the Council of Scientific & Industrial Research (CSIR). A.T. acknowledges research funding support from ANRF (Anusandhan National Research Foundation; Grant #: CRG/2022/003266). M.S. acknowledge research grant support from DBT Wellcome Trust India Alliance Senior Fellowship (IA/S/19/1/504270). S.K. is a JC Bose Fellow of the Department of Science and Technology, India and his laboratory is supported by grants from CSIR, Government of India. V.S. acknowledges the support of Department of Atomic Energy, Government of India, under Project Identification No. RTI 4006 and NCBS-TIFR-core funds. We acknowledge the biosafety level III (BSL3), central imaging and flow cytometry (CIFF), animal care and resource center (ACRC) facilities in NCBS.

Author contributions

A.K., A.T., M.S., S.K., and V.S. helped in conceptualization of findings reported in the manuscript. A.K., N.B., and S.S. designed the study. N.B., S.S., D.A., Ankita S, and M.G. performed the experiments and analyzed data. S.M. helped in conducting animal experiment. Anunay S helped in data analysis and data presentation, especially in preparation of violin plots using ggplot2 tool in R software. A.P.D. helped in conducting and analyzing the ChIP assay. A.K., S.S., and N.B. wrote the manuscript. All authors reviewed the results and approved the final version of the manuscript.

Competing interests

The authors declare no competing interests.

Additional information

Supplementary information The online version contains supplementary material available at https://doi.org/10.1038/s41467-025-64404-z.

Correspondence and requests for materials should be addressed to Ashwani Kumar.

Peer review information *Nature Communications* thanks the anonymous reviewers for their contribution to the peer review of this work. A peer review file is available.